

Cost and Routing of Continuous Variable Quantum Networks

Federico Centrone,^{1,*} Frederic Grosshans,^{2,†} and Valentina Parigi^{3,‡}

¹*ICFO-Institut de Ciències Fotoniques, The Barcelona Institute of Science and Technology, 08860 Castelldefels (Barcelona), Spain*

²*Sorbonne Université, CNRS, LIP6, 4 place Jussieu, F-75005 Paris, France*

³*Laboratoire Kastler Brossel, Sorbonne Université, CNRS, ENS-Université PSL, Collège de France, 4 place Jussieu, F-75252 Paris, France*

We study continuous-variable graph states with regular and complex network shapes and we report for their cost as a global measure of squeezing and number of squeezed modes that are necessary to build the network. We provide an analytical formula to compute the experimental resources required to implement the graph states and we use it to show that the scaling of the squeezing cost with the size of the network strictly depends on its topology. We show that homodyne measurements along parallel paths between two nodes allow to increase the final entanglement in these nodes and we use this effect to boost the efficiency of an entanglement routing protocol. The devised routing protocol is particularly efficient in running-time for complex sparse networks.

I. INTRODUCTION

Networks science has been used to model the structures and properties of many biological, physical and technological systems, including internet and the world wide web. Photonics quantum networks are essential resources for quantum information processing and notably for quantum internet applications, where quantum states of light will allow for the efficient distribution and manipulation of information [1–4]. In order to develop large scale quantum communications and build a quantum internet it is compulsory to grasp the potentialities of quantum networks and exploit all their exceptional features. We can expect that complex networks theory can be used, like in the case of classical networks, to study and drive efficient quantum complex networks design for quantum technologies [5].

In this work we study continuous variable quantum networks in the form of CV graph states with regular and complex topologies. CV quantum information describes quantum states living in infinite dimensional Hilbert spaces, protocols mainly rely on coherent (homodyne) detection which, differently from photon counting detectors, can be highly efficient at room temperature. Moreover, CV quantum networks can be generated deterministically with a large number of nodes [6–10], they can be easily re-configured [11–14] and they have been also exploited in quantum advantage demonstrations [14].

It is known that quantum feature of CV states can be lost because of losses and noise during transmission. Nevertheless substantial progress has been done in CV quantum states distribution [15] and CV quantum repeaters design [16]. Moreover CV quantum networks, that are easily reconfigurable and with a large number of components [7, 8, 10, 14], can be easily exploited as local area quantum networks.

In this work we discuss Gaussian graph states using

mathematical tools from network science in order to estimate how the cost of their experimental implementation is affected by the topology and the size of the network. In particular, we derive an equation providing the squeezing values required to experimentally build a graph state as a function of its graph spectrum. We then adopt a resource theory of squeezing to estimate the cost of expanding the network.

Thereafter, we propose a CV architecture for the quantum internet based on the Gaussian network previously described. We simulate quantum communication protocols through the network by letting the spatially separated agents present at each node perform a homodyne measurement on their optical mode and look for the optimal measurement strategy to maximize the logarithmic negativity — an entanglement measure [17–19] — of the entangled pair shared by the two users who want to communicate, Alice and Bob. We prove that when multiple entangled paths connect Alice to Bob the optimal measurement strategy allows to increase the logarithmic negativity in the final pair. This *parallel enhancement of entanglement* can be used to increase the quality of quantum communications in some selected network topologies.

Lastly, we employ our previous findings to implement a heuristic routing protocol for distributing and boosting the entanglement between two arbitrary agents. The algorithm we provide, on the one hand, is much more efficient than directly checking all possible combinations of quadrature measurements and, on the other hand, it always provides higher logarithmic negativity than the classical scheme, which is directly employing the shortest path between Alice and Bob and neglect the parallel channels.

II. RESULTS

A. Cost of quantum networks

Consider a graph with N vertices. It is fully defined by its adjacency matrix $A \in \mathbb{R}^{N \times N}$. A way to prepare the

* fcentrone@icfo.net

† frederic.grosshans@lip6.fr

‡ valentina.parigi@lkb.upmc.fr

associated graph state is to prepare a mode in the vacuum state for each vertex i and, whenever two vertices i, j are connected by an edge — when $A_{ij} \neq 0$ —, we apply an entangling gate such as a CZ-gate of strength A_{ij} . We then end up with a Gaussian graph state characterized the $2N \times 2N$ covariance matrix σ :

$$\sigma = \frac{1}{2} \begin{pmatrix} \mathbb{1} & A \\ A & \mathbb{1} + A^2 \end{pmatrix}, \quad (1)$$

where we have normalized the vacuum state variance to $1/2$.

These Gaussian bosonic states are of particular significance in the theory of continuous variable quantum information. They are in fact resources for measurement based quantum computing [20, 21], quantum simulations [11], multi-party quantum communication [7, 22], and quantum metrology [23, 24]. Furthermore, their graphical structure simplifies their study through *graphical calculus*, a formalism introduced by Menicucci, Flammia and van Loock in Ref. [25]. Some elements of graphical calculus are summed up in Appendix C.

The correlations between the quadrature measurements of Gaussian states are fully described by their covariance matrix σ . Therefore, as usual in the literature, we will not further mention the first moments, which only describe a deterministic shift of the measurements which can easily be compensated when known and are therefore irrelevant.

Through the Bloch–Messiah decomposition (see Sec. III A), one can see the eigenvalues λ_i^\pm of the covariance matrix σ represent the squeezed and antisqueezed variances of the uncoupled oscillators, e.g. the uncertainty of measuring the real and imaginary part of the electromagnetic field. Together, they form the *squeezing spectrum*. The first result of this paper is the following analytical relation between the squeezing spectrum of the Gaussian state and the adjacency spectrum of the graph:

$$\lambda_i^\pm = \frac{1}{2} \left(1 + D_i^2/2 \pm \sqrt{D_i^2 + D_i^4/4} \right), \quad (2)$$

where D_i are the eigenvalues of the adjacency matrix A . Equation (2) shows the interplay between the physical resources necessary to experimentally implement a CV graph state and the spectrum of the underlying graph. This implies that we can use spectral graph theory to characterize analytically the physical requirements of building Gaussian networks and thus predict which one will be easier to realize. A first crucial consequence is that different graph states whose underlying graphs are co-spectral, e.g. their adjacency matrices have the same eigenvalues, can be transformed into each other applying passive linear optics¹. The intrinsic connection between the squeezing

of a Gaussian network and its topology was already put in evidence in the limit of large squeezing by Gu et al. [21], who showed a relation between the squeezing required to produce a CV graph state and the singular value decomposition of the associated adjacency matrix. Our result is a generalization of theorems 2 and 3 of Ref. [21], exact and valid for finite squeezing, i.e. in a regime accessible with current technology.

Another crucial consequence of equation (2) is that for CV graph states the number of independent squeezed modes in their Bloch–Messiah decomposition corresponds to the rank $\text{rk}(A)$ of the associated adjacency matrix A . This immediately translates to the number of squeezers needed to construct said state.

Squeezing is the essential resource for building Gaussian entangled states. A natural question is thus: what is the squeezing cost of producing a quantum state? A general resource theory for Gaussian states is provided by Lami et al. in [26], with the specific case of squeezing described in [27], where Idel, Lercher and Wolf find an operational squeezing measure, the *squeezing cost*. Its expression for any pure² Gaussian state of covariance matrix σ is

$$G : \mathbb{R}^{2N \times 2N} \rightarrow \mathbb{R}, \quad G(\sigma) = \sum_{i=1}^N 10 \log_{10} (2\lambda_i^+(\sigma)), \quad (3)$$

where we chose to express it in dB.

We employ this to classify networks topologies, depending on the scaling of their squeezing cost with the size of the network. In the following, we will consider an initial set of N modes vacuum states with no squeezing ($s = 0$), as it can be easily proved that initial uniform squeezing only adds a constant factor to the final squeezing cost. We also assume that the CZ-gate coupling strength $A_{ij} = g = 1$ for every edge of the graph, keeping the effects of non-uniform correlations for future works.

1. Regular networks

Let us first discuss some regular network structures by taking a look at the full squeezing spectrum of these topologies — defined in Sec. II B 1 — for a fixed number of nodes $N = 100$. This is shown in figure 1, where the values have been computed from the adjacency matrix spectrum of regular graphs [28]. We can see that, as expected, the linear and the ring graphs have a very similar spectrum, with small deviations induced by the periodicity of the latter that becomes negligible for large N . The star and the diamond networks only have two identically squeezed modes for all N . They are thus

¹ In general, any CV graph can be reshaped in any other graph via a symplectic transformation; in this case it is an orthogonal transformation, and its physical realization involves only linear optics without any supplementary squeezing.

² The more generic expression for mixed states is slightly more involved : $G(\sigma) = -\sum_{i=1}^N 10 \log_{10} \left[\max \left(2\lambda_i^-(\sigma), 1 \right) \right]$. For pure Gaussian states —i.e. all the states considered in this work —, this expression is equivalent to Eq. (3) because $\sqrt{\lambda_i^+ \lambda_i^-} = \frac{1}{2}$.

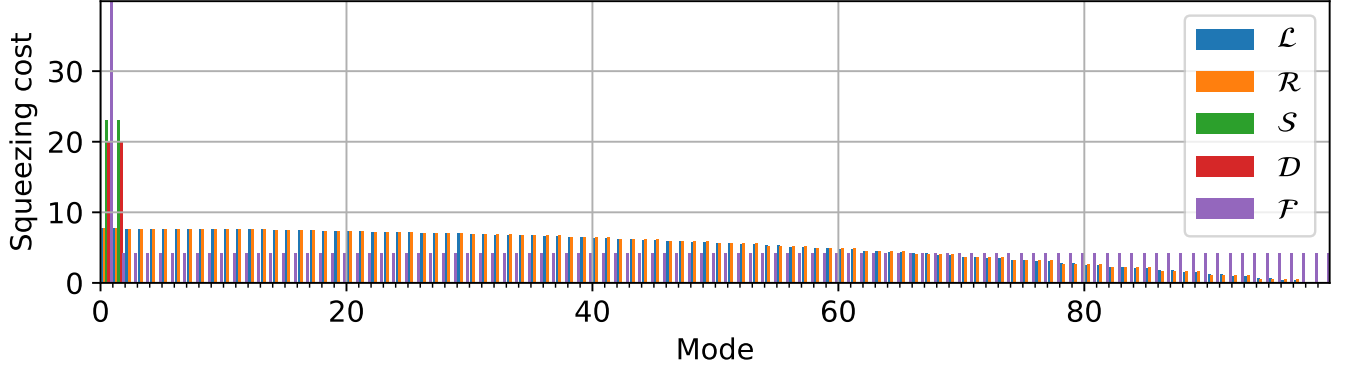


FIG. 1: Squeezing cost distribution for the regular networks defined in Sec. II B 1: linear \mathcal{L}_N , ring \mathcal{R}_N , star \mathcal{S}_N , diamond \mathcal{D}_N , fully connected \mathcal{F}_N networks in the $N = 100$ supermodes, $s = 0, g = 1$. All the networks present some squeezing in each mode except the \mathcal{S} and \mathcal{D} that have an equal amount of squeezing only in the first two modes. The \mathcal{F} network has a large peak of squeezing in the first mode, while the remaining amount of squeezing is equally distributed in the other modes.

co-spectral up to a factor and can be transformed into each other with linear optics. Finally, the fully connected graph has one large eigenvalue that grows with N and $N - 1$ equal eigenvalues, independent of the size of the graph. These eigenvalues are computed analytically by diagonalizing the adjacency matrix A and using Eq. (2) in Appendix A.

Let us now see how the total squeezing cost $G(\sigma)$ scales with the number of nodes N for each of the network topologies presented above. This scaling is computed analytically using Eq. (3) in appendix A. In Fig. 2 we can see

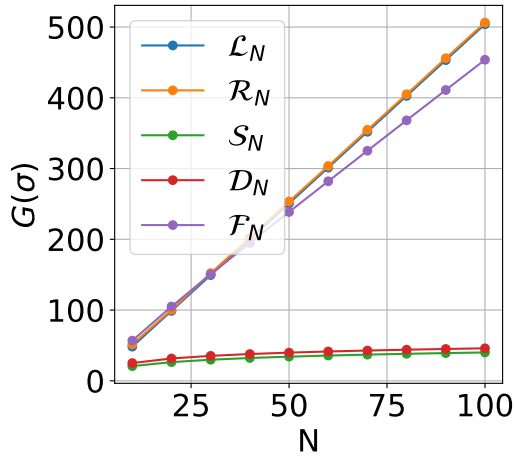


FIG. 2: Trend of the squeezing cost $G(\sigma)$ for the regular topologies: linear \mathcal{L}_N , ring \mathcal{R}_N , star \mathcal{S}_N , diamond \mathcal{D}_N , fully connected \mathcal{F}_N networks for $N = 100$ nodes.

how the linear graph in blue and the ring graph in orange are superposed, sharing the same squeezing cost per node that, as shown in appendix A, is constant with N . The cost of the star and diamond grows logarithmically with N and in both cases has a simple expression and present the lowest cost among the regular graphs we studied. In all these cases, although the actual squeezing cost would

be smaller for these networks, the amount of squeezing required in each mode is much larger so, depending on the experimental scenario, their implementation could be the easiest or the most challenging from an experimental point of view. In any case, these networks have interesting applications for quantum communications. In particular, the star graph can be used for secret sharing [7], while the diamond produce an effect that we called *parallel enhancement of entanglement*, which will be explained in the next section. Finally, the fully connected graph, has a cost that grows linearly with N and, despite having the largest number of edges and thus of squeezing increasing operations, for a large number of nodes is slightly cheaper than the linear graph.

A relevant application of these results would be to minimize the experimental difficulty — modelled by the squeezing cost and/or the number of squeezers — to prepare the Gaussian graph states used as resource for universal quantum computation. To our knowledge, all such proposals rely on 2D-lattice structures [20, 21], similar to the ones proved to be necessary in DV measurement-based quantum computation [29]. We show in appendix A the squeezing cost of a D dimensional cubic lattice to scale linearly with the number of qumodes they contain. We conjecture the same proportionality holds for any D -dimensional regular lattice. Furthermore, we conjecture this cost is proportional to the number of qubits used for the equivalent DV measurement-based quantum computation [29], which is itself proportional to the spacetime complexity of the corresponding quantum computation in the circuit model.

2. Complex networks

Complex networks are important in many natural and technological systems [30]; similarly CV graph states with complex networks shapes are particularly relevant for simulating quantum complex networks environments [11, 31]

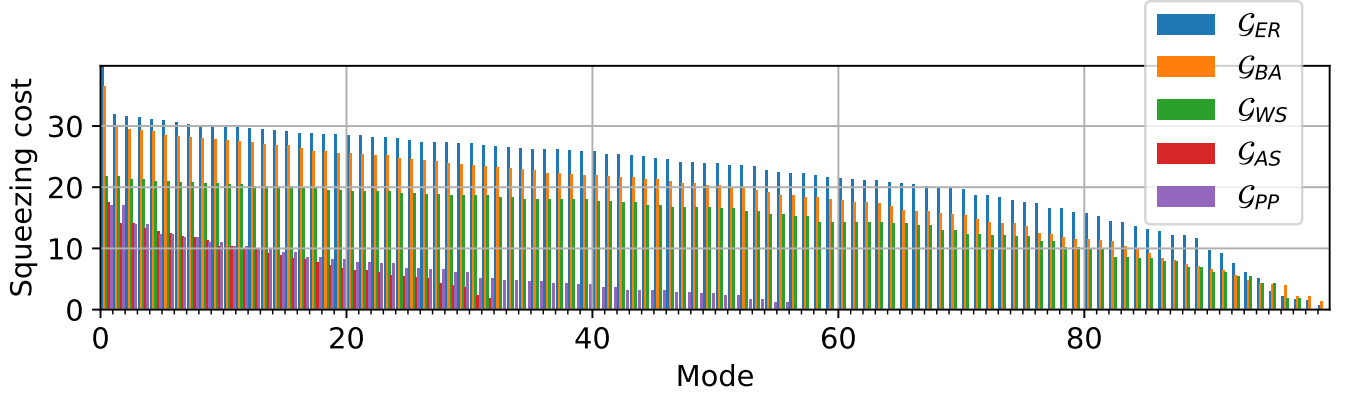


FIG. 3: Squeezing cost distribution for complex topologies: Erdős-Rényi \mathcal{G}_{ER} , Barabási-Albert \mathcal{G}_{BA} , Watts-Strogatz \mathcal{G}_{WS} , AS internet \mathcal{G}_{AS} and Protein-Protein interaction \mathcal{G}_{PP} networks in the $N = 100$ supermodes.

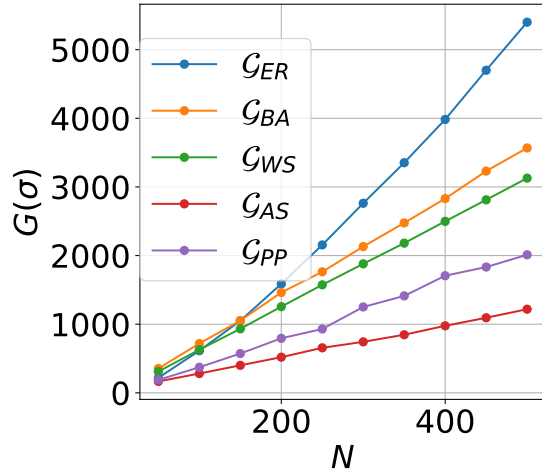


FIG. 4: Trend of the squeezing cost for complex topologies: Erdős-Rényi \mathcal{G}_{ER} , Barabási-Albert \mathcal{G}_{BA} , Watts-Strogatz \mathcal{G}_{WS} , AS internet \mathcal{G}_{AS} and Protein-Protein interaction \mathcal{G}_{PP} networks up to $N = 500$ nodes.

and to study future quantum information/communication networks mimicking the structure of the classical communication networks. It is then worth to study the scaling of the necessary squeezing resources for their implementation. In Fig. 3 we show the squeezing cost distribution for the various topologies of complex networks by showing the squeezing cost of all the principal modes. Notice that, since complex networks are a subset of correlated random networks, the set of eigenvalues of the adjacency matrix is not deterministic. However, the eigenvalues follow a probability distribution $f(x)$ — well known in some selected cases [32] —, which allows to derive the expectation value of the total squeezing cost as

$$\langle G(\sigma) \rangle = 10N \int f(x) \log_{10}[\lambda^{(+)}(x)] dx, \quad (4)$$

where $\lambda^{(+)}(x)$ is the largest eigenvalue deduced from eq. (2), where x is the real random variable describing the

eigenvalues of the (random) adjacency matrix A . This gives us a straightforward recipe to compute G from the distribution f . Furthermore, it allows us to deduce the scaling of G from the distribution of the eigenvalues and especially from the width of this distribution. In fact, if the distribution does not change with N , then G scales linearly with N , whereas any growth in the width of f would imply a superlinear scaling of G .

In Fig. 4 we report the trend of the total squeezing cost as a function of the number of nodes for each of the above complex topologies. In this case, the networks were simulated and the values obtained were averaged over ten different samples.

From the plots we notice that the linear trend is the most common case. The spectral theory of real graphs is a much less established field and there is only a handful of results we can apply to actually make predictions. In particular, to the best of our knowledge there are only empirical results about the convergence of the spectral density for the scale-free and the small-world models. In Ref. [32], however, Farkas et al. show some crucial properties of the spectra of scale-free and small-world graphs, although further studies are required in order to have a deeper insight in the properties of complex quantum graph states. In particular, it is shown that, fixing the other network's parameters, the width of their distribution is constant with N , implying as we discussed a linear trend of G , consistent with the observed one.

The protein-protein [33] and Autonomous System networks, which are scale free networks, have the additional property of having many nodes sharing the same neighborhood which implies a large kernel of their adjacency matrix and thus a slower growth of G compared to the other complex graphs, which are essentially full rank. More specifically, the low rank of the protein-protein interaction graph of Ispolatov, Krapivsky and Yuryev [33], is explained by the duplication process at the heart of its generation, which, by definition duplicates the neighborhood of vertices. For the Autonomous System graph — a model of internet by Elmokahfi, Kvalbein and Dovrolis

[34] —, many of the nodes are leafs (clients) connected to a few client providers. This results in a very low — but still linearly increasing with N — rank, explaining why its squeezing cost is the lowest of the line in Fig. 4.

The anomalous superlinear trend of the ER model is actually a direct consequence of the same theory. As we show in appendix B, this $N \log N$ scaling is due to the widening with N of the Wigner semi-circular law [35] followed by the ER graph.

Now that we have characterized the cost of implementing Gaussian quantum networks, we will describe how to use them as a substrate to perform quantum communications.

B. Routing entanglement

Quantum entanglement is a paramount resource for quantum information purposes. In particular, bipartite entanglement represents the fundamental requirement that a shared quantum channel should have in order to enable a truly quantum teleportation. In the framework of Quantum Communications, the networks previously described can be seen as distributed Gaussian *quantum teleportation networks* [36], where each pair of nodes can employ the pre-established quantum correlations together with *Local Operations* and *Classical Communications LOCC* to teleport a Gaussian quantum state from one node to the other.

In our framework, if two nodes A and B need to teleport a quantum state, they can be helped by the other nodes in the network who will perform either a quadrature measurement in one of the two complementary canonical variables \hat{q} or \hat{p} in order to increase the strength of the entanglement in the final pair. As detailed in Sec. IV, these two measurements have the effect of either removing the target node and its connections from the network or to wire shorten all its neighbors, respectively.

1. Regular networks

In Fig. 5 we compare the effect of different regular topologies of quantum networks with the purpose of distributing entanglement between two of the furthest nodes inside the network.

The decrease of entanglement with the size of the network seem to be typical in all configurations except the diamond graph, where all the central nodes are \hat{p} -measured. This behaviour is quite counter-intuitive and might be expected to increase the fidelity of quantum communications. We show in Appendix D the lowest symplectic eigenvalue of the partially transposed covariance matrix for this system goes like

$$\left(\nu_-^{(\mathcal{D}_N)}\right)^2 = \frac{1}{1 + 2NRg^2}, \quad (5)$$

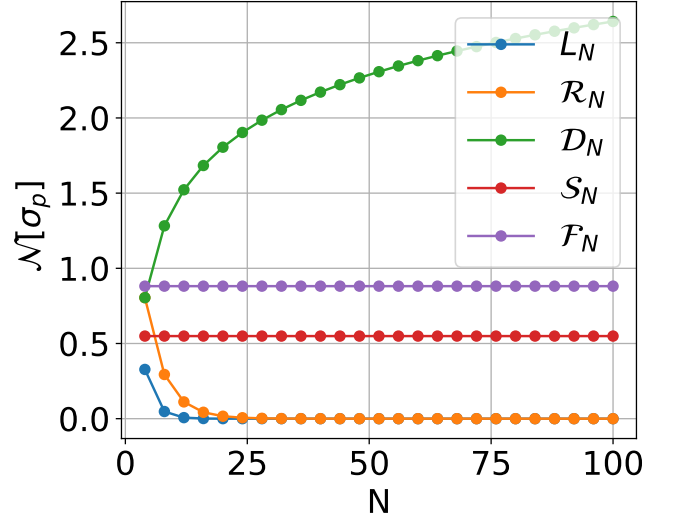


FIG. 5: Logarithmic negativity in the final two modes states after that all the other agents have locally measured their node for the regular topologies: linear \mathcal{L}_N , ring \mathcal{R}_N , star \mathcal{S}_N , diamond \mathcal{D}_N , fully connected \mathcal{F}_N networks up to $N = 100$ nodes.

Where $R = 10^{s/10}$ is the inverse of the squeezing in \hat{p} , with squeezing factor s in dB. Hence, the logarithmic negativity grows logarithmically with NRg^2

$$\mathcal{N}^{(\mathcal{D}_N)} = \log_2(1 + 2NRg^2), \quad (6)$$

and the two modes become perfectly correlated in the limit of either infinite squeezing, infinite strength CZ-gate or infinitely many nodes in the network.

2. Complex networks

We present a naïve entanglement routing protocol that takes into account some of the properties studied in the previous section (notably, the parallel enhancement of entanglement) and we will apply it to complex topologies, to show that the enhancement of the entanglement with respect to the trivial protocol is, in principle, easily achievable. Imagine we have a distributed network of entangled harmonic oscillators, where each node is honest and can perform classical communication and local homodyne measurement, and we want to establish an entangled pair between two nodes, Alice and Bob, that want to teleport a quantum state or perform QKD. The trivial protocol — called *Shortest* in the following — would be to find the shortest path between them and measure in \hat{p} all the qumodes along this path and in \hat{q} all the others. A careful look at the inner structure of the network, however, might help us increase the strength of the correlation. For example if at any point, two nodes on the path are linked by multiple parallel routes, we can measure these in \hat{p} to exploit the parallel enhancement of this Diamond-like subnetwork.

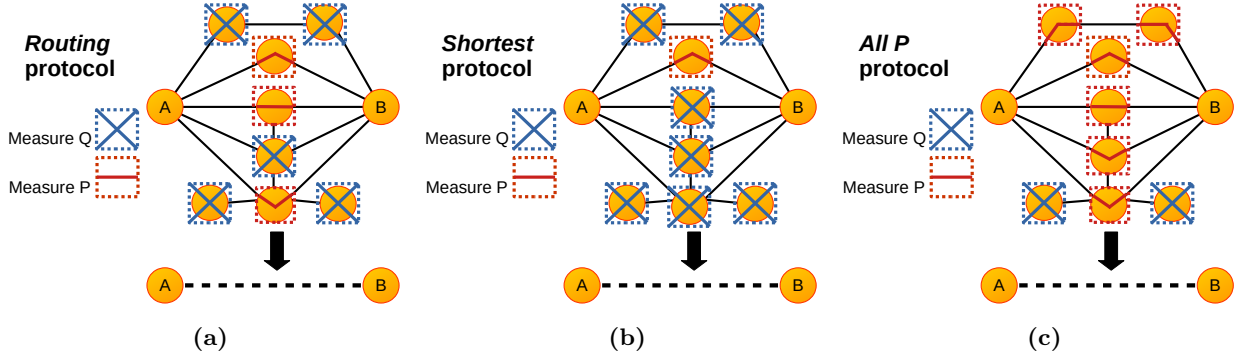


FIG. 6: Scheme of the three protocols for the entanglement distribution: (a) the *Routing* protocol takes a list of the shortest paths connecting A and B and measures in \hat{p} those that increase the logarithmic negativity while the rest is measured in \hat{q} ; (b) the *Shortest* protocol only consider one of the shortest paths to be measured in \hat{p} and the rest in measured in \hat{q} ; (c) the *All P* measures the nodes with only one connection in \hat{q} and all the rest in \hat{p} .

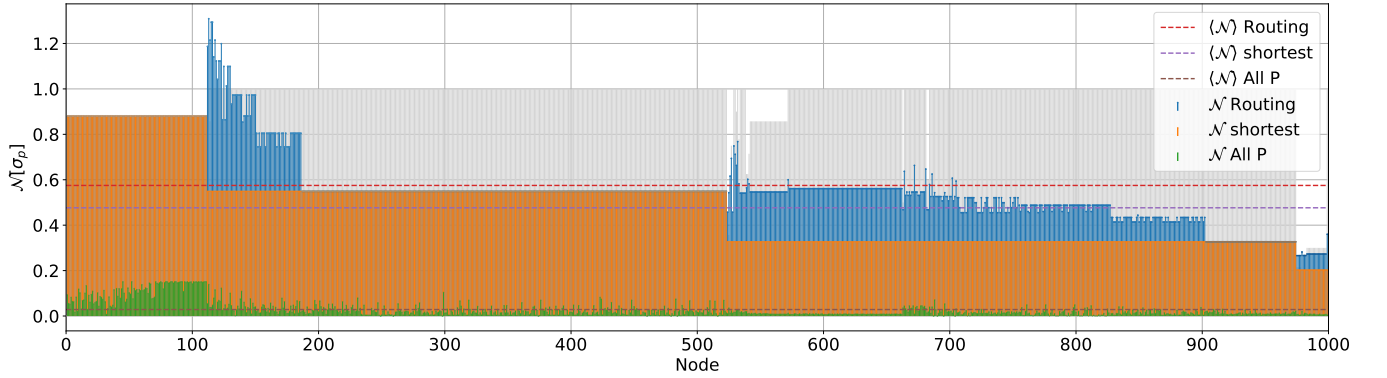


FIG. 7: Logarithmic negativity produced by the three different protocols applied to each node of the the Autonomous System $\mathcal{G}_{AS}(N = 1000)$ network. The nodes are labeled in order of distance and of number of paths connecting to Alice. The blue, orange and green stems represent the logarithmic negativity of the final pair after the *Routing*, *Shortest* and *All P* protocols respectively, while the dashed lines represent the mean value for all the nodes. The color of the marker indicates the distance of the node from A and the grey columns represent the ratio of paths that improved the entanglement in *Routing*.

In order to show this in practice, we test the performances of three different routing protocols (shown in figure 6) on various complex networks with the purpose of establishing a highly entangled pair [37]. We choose Alice to be one of the hubs of the graph and evaluate the efficiency of the protocol in delivering entanglement to all the other nodes. The quantum protocol that we propose to exploit the parallel enhancement of entanglement will be simply called *Routing*.

- *Routing*: it takes as input the target node, Bob; it lists all the shortest paths connecting it to Alice and measures all the nodes that are not in these paths in the \hat{q} quadrature, so that they will not influence the protocol. Among the list of paths it checks one by one those to be measured in \hat{p} in order to maximize the logarithmic negativity \mathcal{N} of the final pair, while the rest will be measured in \hat{q} .

In the *Routing* protocol, in principle, we could have considered as well parallel paths of longer lengths that might have contributed to improve the logarithmic negativity.

However, in practice the only observed effect was the slow down the performances while the entanglement was not increasing for all the cases we considered. The effect of the parallel paths can be appreciated when comparing the logarithmic negativity produced by *Routing* with that produced by *Shortest*.

- *Shortest*: the difference of the latter is that it only exploits one of the shortest parallel paths, directly measuring everything else in \hat{q} .

In some cases the two protocols do not give a substantial difference, either because there are no parallel routes or because these do not help increasing the entanglement; however, in many instances the effects of parallel routing are significant. The last protocol we compare with is *All P*.

- *All P*: it measures in \hat{q} all the terminal nodes of degree 1 — the leaves — and the rest in \hat{p} .

This protocol is less effective than the first two but is always the quickest to simulate, whereas *Routing* can be

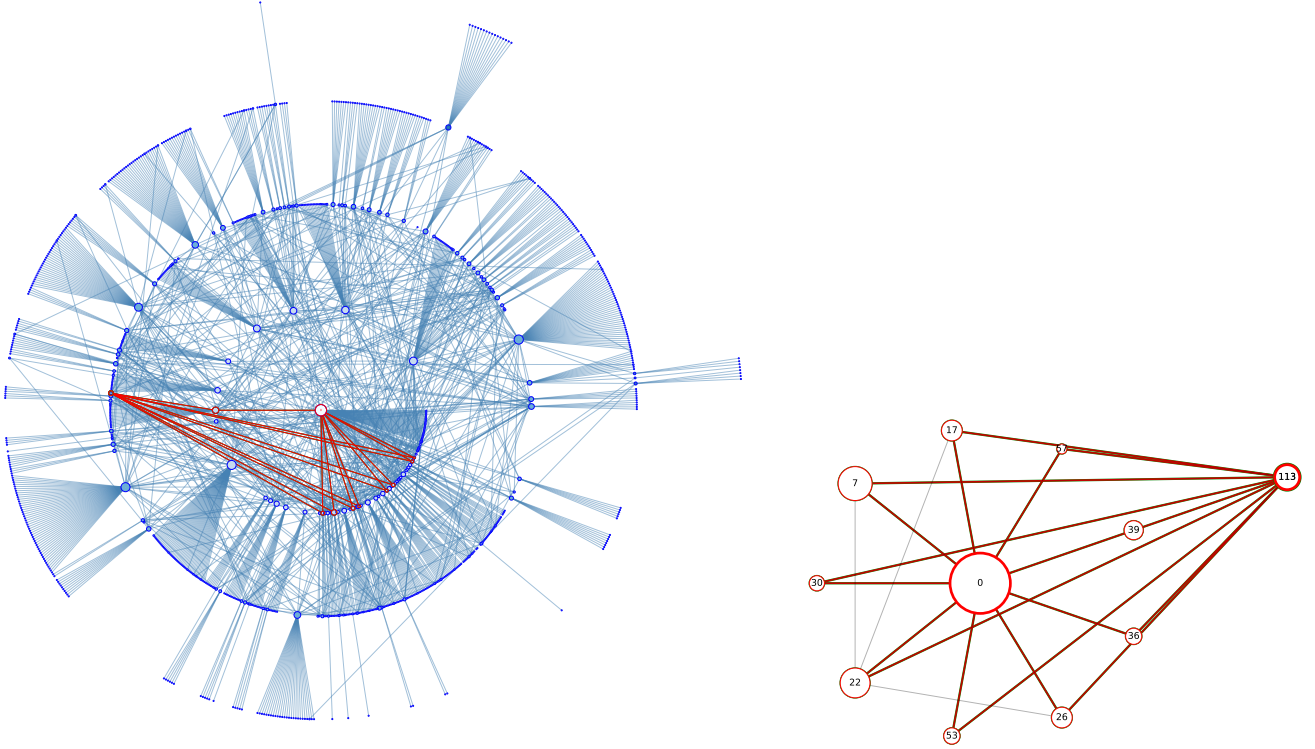


FIG. 8: Scheme of the $\mathcal{G}_{AS}(N = 1000)$ network on which we performed the protocol and subgraph of the paths connecting to the node with highest logarithmic negativity. The nodes are set in circles according to their distance from Alice and their size is proportional to their degree.

computationally very slow on regular networks, which are characterized by long distances and many parallel paths, but becomes very efficient on complex sparse networks. The following simulations can be reproduced using our python code, available at [37].

One instance of this program is given in figure 7 which shows the logarithmic negativity provided by the three different protocols for each node of an Autonomous System network [34] with 1000 nodes $\mathcal{G}_{AS}(N = 1000)$. At the beginning of the protocol, we pick Alice as the node, or one of the nodes, with the highest degree. The nodes are then sorted by their distance from Alice and, for the same distance, by the number of all the shortest paths connecting them to Alice. Additionally, the grey column represents the fraction of parallel paths useful to increase the entanglement. Notice that nodes at distance 1 cannot show any difference between the *Routing* and the *Shortest* protocols, however many nodes at distance 2 present a greater logarithmic negativity than those at shorter distance after the *Routing*. This feature of quantum communication networks, e.g. that two nodes can benefit improved communication if they are at larger distance thanks to the parallel enhancement of entanglement, has no classical equivalent.

In figure 8 we show the graph of the network, where the nodes are again sorted by distance and number of parallel paths and the size of each node is proportional to

its degree. In this figure Alice is ‘0’ and has a thick red contour. The node with highest logarithmic negativity and all the paths that improved its entanglement are highlighted with red thick lines.

Appendix E presents the results of the same analysis we applied to other networks differing in size and topology, and for which we obtained different results.

C. Discussion

Our model aims at reproducing the existing photonic platforms [7, 8, 10, 14] with realistic experimental constraints, such as limited amount of squeezing, but without taking into account propagation losses. This work is focused on the capabilities of pure CV quantum states to act as quantum networks and the resources needed for their generation. Generation losses can be very low, so that the hypothesis of pure states is a realistic one, whereas propagation losses can be mitigated by considering local (short distances) networks, and their effect on long distances will be included in future works. At the same time we probe the capabilities of photonic platforms while the scaling of the network increases beyond the capacities allowed by the state-of-the-art technology. Since the main limitation to build these optical systems is finite squeezing, we provide in section II A an analytical formula that allows

to compute the amount of squeezing in each mode as a function of the spectrum of the underlying graph. We show the graph states' cost as a global measure of squeezing and number of squeezed modes that are necessary to build the network. In particular we explore the cost of different networks topologies in term of number of needed squeezers at fixed number of nodes in the networks and of the global amount of squeezing.

Although in entangled qubits networks the resource usage is always proportional to the number of links, we show that in CV Gaussian networks the trend of the squeezing cost presents non-trivial scaling with the size of the network and this is strictly dependent on its topology. We present as well a few instances of the full squeezing spectra — i.e. the needed amount of squeezers with the required squeezing values — of regular and complex networks, showing that some topologies are equivalent up to a linear optical transformation.

We then explore their potentialities to perform efficient quantum communications between two arbitrary nodes when assisted with a given class of Gaussian Local Operations and Classical Communication (GLOCC) by all the agents in the network. A typical approach of quantum networking and routing consists in distributing photonic states like single-photons, Bell pairs or Gaussian states and then use synchronous local operations that build the wanted entanglement structure between the agents [3, 38–46]. We remark that our type of communication quantum networks is inherently different from the typical qubits networks that are currently being deployed in different metropolitan areas [47]. In those cases, for example, each entanglement link is pairwise between two qubits and as a consequence each node of the network will have to receive, storage and measure as many quantum states as it has neighbors. Conversely, in a Gaussian quantum network the same qumode can be entangled with an arbitrary number of other nodes. Moreover, the production of such states, their manipulation to increase the entanglement among two nodes and their measurement to perform quantum teleportation can be achieved deterministically, unlike the discrete variables case. Nonetheless, qubits networks have been extensively studied over the last years, whereas Gaussian teleportation networks is a very recent emerging field. Our purpose is, thus, not to prove the superiority of the latter, but rather to explore its properties and the differences from the DV schemes in order to get the best of both worlds.

We consider the case where a preexisting CV multipartite entangled state is distributed among the players and then local operations reconfigure the entanglement connections, similarly to some protocol in the DV case [48]. The choice is motivated by the fact that multimode entangled states can be directly generated via optical platform [6, 8–10, 49] and their shape can be easily manipulated [7, 11]. We show, both analytically and numerically that, in specific topologies, homodyne measurements along parallel paths allow to increase the entanglement between two distant nodes.

We discovered some outstanding properties of Gaussian networks. The most important is the parallel enhancement of entanglement in the diamond graph. If properly used, this feature can most certainly improve the routing of entanglement in regular and complex shaped networks. On these grounds, the search for an optimal protocol that exploits all the qualities of these Gaussian networks is very desirable yet arduous, and will be subject of future investigations.

Finally, we devise a routing protocol based on local quadrature measurements for reshaping the network in order to perform a teleportation protocol between two arbitrary nodes of the networks. The *Routing* protocol, which is based on wire-shortening over parallel paths among the nodes, improves the final entanglement between the two nodes in a considerable amount of cases, and it is particularly efficient in running-time for complex sparse networks.

III. METHODS

A. Gaussian quantum states

The generation of continuous variables multimode entangled states has been demonstrated in several optical setups. In such experiments we recover networks structures as naturally appearing entanglement correlations [49], reconfigurable Gaussian interactions [11], or imprinted cluster states [7–10, 50].

These quantum states produced via parametric processes and linear optical transformations are characterized by Gaussian statistical distribution of the quadratures of the involved optical modes [51]. The quadratures \hat{q}_j and \hat{p}_j of the j^{th} mode are canonical conjugate variables, such that $[\hat{q}_j, \hat{p}_k] = i\delta_{j,k}$, associated to the quantum harmonic oscillator describing the light mode. In this work we adopt the following relation with creation and annihilation operators $\hat{\mathbf{a}}^\dagger = (\hat{\mathbf{q}} - i\hat{\mathbf{p}})/\sqrt{2}$ and $\hat{\mathbf{a}} = (\hat{\mathbf{q}} + i\hat{\mathbf{p}})/\sqrt{2}$, such that the variance of the vacuum quadratures is normalized to $1/2$.

The produced states can then be completely characterized by the first two moments of the quadratures $\bar{\mathbf{r}} = \text{Tr}[\rho\hat{\mathbf{r}}]$ and $\sigma = \text{Tr}[\rho\{(\hat{\mathbf{r}} - \bar{\mathbf{r}}), (\hat{\mathbf{r}} - \bar{\mathbf{r}})^T\}]$, where ρ is the density matrix of the Gaussian state and $\hat{\mathbf{r}} = (\hat{q}_1 \dots \hat{q}_N, \hat{p}_1 \dots \hat{p}_N)$ — we follow here qp -ordering.

Parametric processes are described by quadratic Hamiltonians $\hat{\mathcal{H}}_I = \hat{\mathbf{r}}H\hat{\mathbf{r}}^T$, whose dynamics is implemented on the quadratures by $S_H = e^{\Omega H t}$, as

$$\hat{\mathbf{r}}' = S_H \hat{\mathbf{r}}_0 \quad (7)$$

where $\hat{\mathbf{r}}_0$ are quadratures of the initial state, $\hat{\mathbf{r}}'$ are the quadratures of the final state and $\Omega = \begin{pmatrix} 0 & \mathbb{1} \\ -\mathbb{1} & 0 \end{pmatrix}$ is a $2N \times 2N$ skew-symmetric matrix associated to the N dimensional Hilbert space allowing to write the commutation relation of the canonical variables as

$$[\hat{\mathbf{r}}, \hat{\mathbf{r}}^T] = i\Omega = i \begin{pmatrix} 0 & \mathbb{1} \\ -\mathbb{1} & 0 \end{pmatrix}.$$

Since any pure Gaussian state can be obtained by the application of a unitary generated by a quadratic Hamiltonian H to the vacuum, the most general pure Gaussian state covariance matrix is given by applying S_H by congruence to the vacuum covariance matrix $\sigma_0 = 1/2$:

$$\sigma = S_H \sigma_0 S_H^T = \frac{S_H S_H^T}{2} \quad (8)$$

Singular value decomposition allows one to write the symplectic transformation in the so called Bloch-Messiah decomposition [51] as a product of an orthogonal, a diagonal and an orthogonal matrices $S_H = O \Delta O'$, which can be interpreted as a basis rotation, a squeezing in the diagonal basis and another rotation. The mode-basis in which the covariance matrix is diagonal and each component is independently squeezed is named the supermode basis. In [7, 49] where the pump and the phase matching function can be described by a Gaussian spectral profile, the supermode basis corresponds to Hermite-Gauss spectral modes. The squeezing values of Δ can be derived from the eigenvalues of the Hamiltonian $\hat{\mathcal{H}}_I$, while the orthogonal matrix O can be interpreted as a measurement basis change or, equivalently, as a passive linear optical transformation. The other orthogonal matrix O' is simplified in the product $S_H S_H^T$ and can be disregarded:

$$\sigma = \frac{S_H S_H^T}{2} = \frac{1}{2} O \Delta^2 O^T. \quad (9)$$

The diagonal matrix Δ contains the information on the minimum number of squeezed modes in the system and their value of squeezing, which will later be used in the chosen resource theory. If we consider a single mode field, the squeezing operation is defined as a Gaussian transformation that reduces the variance of \hat{p} by a factor $10^{-s/10}$, where s , measured in dB throughout this article, is called *squeezing factor*. Squeezing is represented by the local symplectic matrix

$$S_{sq}(s) = \begin{pmatrix} 10^{s/20} & 0 \\ 0 & 10^{-s/20} \end{pmatrix}.$$

The multimode Δ matrix can then be written as

$$\Delta = \text{diag}\{10^{s_1/20}, 10^{s_2/20}, \dots, 10^{s_N/20}, 10^{-s_1/20}, 10^{-s_2/20}, \dots, 10^{-s_N/20}\}. \quad (10)$$

This formalism can be used to visualize and manipulate Gaussian quantum states, that are readily available in most well-equipped photonics laboratories and, although the number of modes and their connections is still in large part limited, many efforts are employed to improve the capacities of these systems.

Targeted Gaussian quantum states, including the quantum networks of the next section, can be generated via the two following strategies: i) by tailoring Hamiltonians $\hat{\mathcal{H}}_I$ of multimode parametric processes in order to get the decomposition of eq. (9) corresponding to the desired

covariance matrix [6, 7, 52–55]; ii) by getting a number of single-mode squeezers equal to the number of elements with $s_j \neq 0$ of Δ in eq. (9) and producing the corresponding s_j squeezed states, that are injected in a linear optic interferometer corresponding to the orthogonal matrix O in eq. (9) [56–58].

B. Graph states as quantum networks

The above formalism can be employed to describe Gaussian graph states, that can be used as CV quantum networks. We at first recall that a network is mathematically described by a graph $\mathcal{G}(V, E)$, which is a set of vertices V (or nodes) connected by a set of edges E . Labeling the nodes of the graph in some arbitrary order, we can define a symmetric adjacency matrix $A = A^T$ whose $(j, k)^{\text{th}}$ entry A_{jk} is equal to the weight of the edge linking node j to node k (with no edge corresponding to a weight of 0). Typically, the adjacency matrix is enough to completely characterize a graph, however we will see that in our case there are other degrees of freedom such as the squeezing of a node and its angle.

We can now describe the quantum networks we use in this work that are called graph- or cluster-states³ [20, 21, 25]. Theoretically, they can be built by entangling a number of squeezed modes of light via CZ-gates, which is a Gaussian operation implementing a correlation of strength g between the \hat{q} and the \hat{p} of the two modes on which it acts. The corresponding symplectic matrix is

$$S_{C_z}(g) = \begin{pmatrix} 1 & 0 & 0 & 0 \\ 0 & 1 & 0 & 0 \\ 0 & g & 1 & 0 \\ g & 0 & 0 & 1 \end{pmatrix}$$

The graph associated to the graph states identify edges as CZ-gates applied between nodes, that are the squeezed modes, weighted with g .

In order to simplify the many degrees of freedom present in our networks, for the moment we shall assume that all the nodes will be squeezed in \hat{p} by s and all the edges have a correlation strength of g . If we apply a CZ-gate network with adjacency matrix A to a multimode squeezed vacuum σ_s , with squeezing factor s we obtain a Gaussian network with covariance matrix [59]

$$\begin{aligned} \sigma &= \begin{pmatrix} \sigma_{qq} & \sigma_{qp} \\ \sigma_{pq} & \sigma_{pp} \end{pmatrix} = \begin{pmatrix} \mathbb{1} & 0 \\ A & \mathbb{1} \end{pmatrix} \sigma_s \begin{pmatrix} \mathbb{1} & A \\ 0 & \mathbb{1} \end{pmatrix} \\ &= \begin{pmatrix} R\mathbb{1} & RA \\ RA & RA^2 + \mathbb{1}/R \end{pmatrix} \end{aligned} \quad (11)$$

Where $R = 10^{s/10}$. The $2N \times 2N$ covariance matrix σ is divided in four $N \times N$ blocks, where the blocks σ_{qq}

³ While usually the name cluster is used when the graph shape allows for universal quantum computing, in this work we will use the terms cluster state and graph state as synonyms.

and σ_{pp} represent the correlations among the different nodes' q - and p -quadratures, respectively, whereas the blocks σ_{qp} and σ_{pq} describes the correlations between q - and p -quadratures.

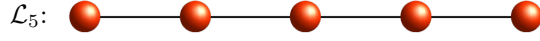
Bear in mind that the *CZ-gate* operations that theoretically identify the edges of the networks are seldom realized in any laboratory being very challenging to accomplish. What is commonly done, as explained in the previous subsection, is the reduction of the covariance matrix of the graph state in (11) to the form of eq. (9), that is also a recipe for building the graph states from a certain number of squeezed modes (Δ) and linear optics transformations (O).

C. Networks

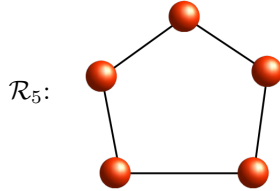
1. Regular topologies

Regular networks are generated through a deterministic mechanism. We considered the following topologies:

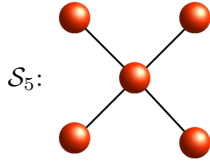
- The *linear graph* \mathcal{L}_N , with N nodes and $N-1$ edges, is accomplished by connecting each node in series to the next.



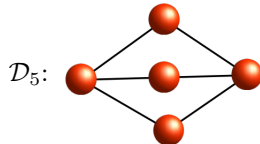
- The *ring graph* \mathcal{R}_N , with N nodes and N edges, is a linear graph with a closed loop.



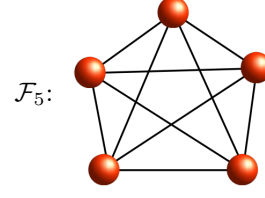
- In the *star graph* topology \mathcal{S}_N , with N nodes and $N-1$ edges, every peripheral node is linked to a central node, called hub.



- The *diamond graph* \mathcal{D}_N , with N nodes and $2(N-2)$ edges, has 2 hubs, each linked to all the $N-2$ central nodes of the network. It is isomorphic to the complete bipartite graph in which one of the subset has 2 nodes and the other has $N-2$ nodes.



- In the *complete* (or *fully connected*) graph \mathcal{F}_N , with N nodes and $\frac{N(N-1)}{2}$ edges, all nodes are interconnected.



The experimental squeezing cost of these graphs was studied in II A 1.

Notice that there is as well a simple relation between the adjacency matrix A of a graph state and the mean energy difference between the state and the vacuum. In fact, assuming that the energy E of the state is the mean value of the harmonic oscillator Hamiltonian on the state

$$E = \langle \hat{H}_{HO} \rangle = \frac{\hbar}{2} \sum_i \omega_i (\langle \hat{x}_i^2 \rangle + \langle \hat{p}_i^2 \rangle) = \frac{\hbar\omega}{2} \text{Tr}(\sigma), \quad (12)$$

where we also assumed that all the modes have the same frequency $\omega_i = \omega$. From this we can write

$$\Delta E = E - E_0 = \frac{\hbar\omega}{2} \text{Tr}(\sigma - \sigma_0) = \frac{\hbar\omega}{2} \text{Tr}(A^2). \quad (13)$$

The quantity on the right hand-side is proportional to the second moment of the eigenvalues distribution and it sets a fundamental lower bound on the energy necessary to implement such states. From a topological point of view, the trace of the n th power of the adjacency matrix equals the number of closed loops of length n on the graph [60]. Thus, for $n=2$, it corresponds to the number of edges in the network and implies that each independent application of the CZ-gate adds the same amount of energy. A resource scaling that is linear with the number of edges in the network is typical of DV networks (i.e. DV graph states), where each new edge requires a new Bell pair. The scaling of the squeezing in CV networks with the size of the network, as we have seen, depends instead on the structure of the underlying graph and can be non-linear with the number of edges. We want to stress here that squeezing — and not energy — is the technologically not-trivial enabling resource to be implemented for building the CV networks. If we look again at the example of the star and the diamond graph, the number of edges in the two graphs are different, hence they would have different energies. As they have the same number of squeezed mode, we can transform one into the other with passive optics, e.g. without spending energy. However, it has to be clarified that the two main squeezed modes for the diamond have larger eigenvalues than the star network. Thus, if we transform a star graph into a diamond with linear optics, it would be equivalent to a graph state obtained by the application of CZ-gate with a weaker coupling g . But again this behaviour is totally accounted by the squeezing cost, which is the relevant quantity in designing CV networks.

2. Complex topologies

In the previous section we described graphs that are built through a deterministic algorithm, though we can also construct a graph based on statistical models [61, 62]. This is the difference between regular and random networks. An exemplary standard for random networks is the Erdős–Rényi model $\mathcal{G}_{ER}(N, p)$, in which each pair of the N nodes have a probability p to be linked; the network thus has $\binom{N}{2}p$ edges on average [63].

Most of the network properties observed in nature, however, simply cannot be described by regular or random graphs. For this reason, a youthful branch of scientific research is committed to the study of *complex networks*. In the field of network theory, complex networks are a type of graphs with non trivial topological features, that are shared by neither regular nor completely random graphs, but are rather akin to networks modeling real systems [30].

An important class of complex networks is characterized by the *small world* property. These networks exhibit the peculiarity of having a low average path length, which is the mean distance between two arbitrary nodes, and a high clustering, which is a measure of the degree to which nodes in a graph tend to cluster together. The emblematic network presenting these features is the Watts–Strogatz model $\mathcal{G}_{WS}(N, Q, \beta)$ [64]. In this model, we first construct a regular periodic graph with N nodes and $\frac{NQ}{2}$ edges where each node has exactly Q neighbors, then with probability β we rewire each edge with another node chosen uniformly at random while avoiding self loops and link duplications.

The second relevant class of complex networks present the typical aspect of being *scale-free* and having *long-tailed* structures. Scale-free networks show a power law in the degree distribution $P(k) \propto k^{-\gamma}$ for some $\gamma > 0$, which is self-similar at all values of k in the *tail* of the distribution, unlike the ER and WS models that go to zero very quickly and have no tails. This fractal like attribute is well reproduced by the Barabási–Albert model $\mathcal{G}_{BA}(N, K)$, which can also emulate growth and preferential attachment in networks [65]. The graph is built sequentially by adding one node at a time and wiring it to K other nodes with a probability that is proportional to the number of links that the target node already has. While adding one node at a time, the first K nodes initially will not be linked to anything, hence this graph will result having $(N - K)K$ edges, mostly connected to a great hub. This type of graph is the canonical example to reproduce some properties of the *World Wide Web*. A particular case of the Barabási–Albert network is the *Tree-graph* $\mathcal{G}_T(N) = \mathcal{G}_{BA}(N, 1)$.

Another notable class of complex networks is constituted by *technological networks*, artificial networks designed typically for distribution of some merchandise or resource, such as electricity or information. The most famous example in this category is the Internet Autonomous System (AS) [34] $\mathcal{G}_{AS}(N)$, the physical global computer

data network. In order to study this topology we will base on the work put forward in ref. [34].

All the complex networks mentioned so far are meant to emulate man-made structures, however complex topologies appear in nature in the most surprising ways. There is a large variety of *biological networks*, among these we will consider specifically the protein–protein interaction network model $\mathcal{G}_{PP}(N, \sigma)$ developed in Ref. [33].

IV. QUANTUM TELEPORTATION GAUSSIAN NETWORKS

In a naïve strategy, the teleportation between two arbitrary nodes can be implemented simply by ignoring all the other nodes and exploiting the residual bipartite entanglement together with classical communications. This strategy is a direct extension of the standard teleportation protocol from two to more stations and is called *non-assisted* protocol [66].

Another set of strategies is based upon a cooperative behavior, where all the other nodes assist the teleportation between the chosen pair (Alice and Bob) by means of LOCC. In fact, if the external nodes perform suitable local measurements and then classically communicate their outcomes to Bob, the latter can use this additional classical information to improve the process via modified conditional displacements. These strategies are called *assisted* protocols and are the ones that determine what we call routing protocol in this Article.

According to Gu et al. [21] quadrature measurement on a mode of a Gaussian network like the ones we considered so far can be described by two simple rules:

- *Vertex Removal*: a \hat{q} -measurement on a qumode removes it from the network, along with all the edges that connect it.
- *Wire Shortening*: a \hat{p} -measurement on a qumode is just a \hat{q} -measurement after a Fourier Transform, which corresponds to a phase rotation of $\pi/2$: $S_F = S_R(\theta = \frac{\pi}{2})$. The node will thus be removed but the phase shift will induce correlations between the neighboring edges. Thus, measurements in the momentum basis allow us to effectively “shorten” linear graph states.

These rules are exposed more formally in Appendix C, using the graphical calculus introduced by Menicucci, Flammia and van Loock [25].

If two nodes A and B need to teleport a quantum state, they can be helped by the other nodes in the network who will perform these operations in order to increase the strength of the entanglement in the final pair. A typical measure of entanglement is the *logarithmic negativity* [17–19, 67]

$$\mathcal{N} = -2 \log_2 \nu_- \quad (14)$$

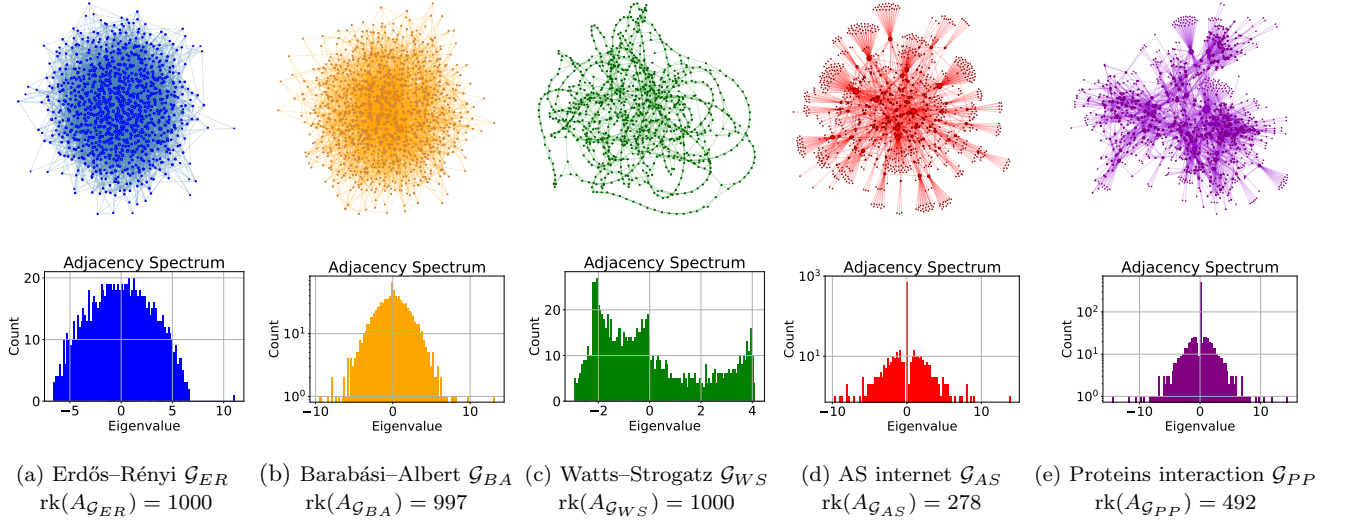


FIG. 9: Some complex networks, their adjacency matrix eigenvalues distribution and the rank of their adjacency matrix for $N = 1000$ nodes. In the distributions of the BA, AS and PP the y-axis is in log-scale.

Where ν_- is the smallest symplectic eigenvalue of the partially transposed covariance matrix of the pair. Partial transposition is a necessary operation for the PPT criterion [68] and is easily implemented in Gaussian states by changing the sign of the momentum of one of the two subsystems.

The symplectic eigenvalues ν_{\pm} of a two-mode system can be computed through the invariants of the covariance matrix [67]. More specifically, we can define the *seralian*

$$\Delta = \det \sigma_A + \det \sigma_B + 2 \det \sigma_{AB}, \quad (15)$$

where σ_A and σ_B are the local covariance matrices of the single-mode sub-systems A and B, and σ_{AB} represents their correlations. From this we can compute the symplectic eigenvalues as:

$$\nu_{\pm}^2 = \frac{\Delta \pm \sqrt{\Delta^2 - 4 \det \sigma}}{2} \quad (16)$$

V. CONCLUSION AND OUTLOOK

In this work we have investigated Gaussian multimode graph states with regular and complex topologies and studied their potential application for quantum communication protocols.

Firstly, we have shown analytically and numerically that the cost of the networks is in general nonlinear with the number of edges and nodes and there are particular (regular and complex) graph shapes that optimize the cost and the number of squeezers over number of nodes and edges in the networks. Among regular networks the diamond and the star graph need only two squeezed nodes to be built, independently from their number of nodes. Among the complex networks shapes, the Internet Autonomous System model is the most convenient in number of needed squeezed states [34].

Then, we have studied the assisted teleportation protocol in Gaussian entangled networks, where couple of nodes are assisted in the teleportation by local measurement in all the other nodes. This naturally define a routing protocol in Gaussian networks. In particular we have considered \hat{q} and \hat{p} homodyne quadrature measurement that allow respectively for vertex-removal and wire-shortening. We showed analytically the effect of parallel enhancement of entanglement to improve the quality of quantum communication in the diamond network.

Finally, inspired by this quantum effect, we have devised a routing protocol that exploits wire shortening in parallels paths and we have applied it to complex networks graphs. The protocol named *Routing* is compared with *Shortest*, where wire shortening is done only in the shortest path, and *All P*, which removes all the terminal nodes while it wire-shorten all the others. In most cases, the *Routing* improves the entanglement compared with *Shortest*. Also, in terms of computational complexity, the *Routing* is much slower than *All P* in regular networks, where there are long distances between nodes and several parallel paths, but it is very efficient in complex sparse networks.

The devised *Routing* protocol is very general so that it can be applied to arbitrary networks, and it is particularly efficient for sparse not regular networks. Our simple graph exploration approach would be improved in computational efficiency by real graph-based algorithms, especially if we allow for approximate solutions [69]. Also it would be interesting to allow for non uniform distributions of squeezing s and CZ-gate strength g or more general homodyne measurements, i.e. going beyond the two \hat{p} and \hat{q} cases and considering measurements along $\hat{q}_{\theta} = \cos(\theta)\hat{q} + \sin(\theta)\hat{p}$. In addition, it could be interesting to examine a scenario in which the intermediate nodes are dishonest and do not cooperate to perform the routing,

exploiting, for example, non-Gaussian operations. Finally the routing protocol has been implemented to solve the particular task of creating a perfect EPR pair between two nodes, future protocols will consider general reshaping in arbitrary multiparty states.

VI. ACKNOWLEDGEMENTS

We thank Dimitrios Tsintsilidas for helpful discussions. This work is supported by the European Research Council under the Consolidator Grant COQCOoN (Grant No. 820079), by the European Union under the project 101080174 CLUSTEC, by the French state from the Plan France 2030 managed by the Agence Nationale de la Recherche through the ANR-22-PETQ-0006 NISQ2LSQ and the OQuLus projects, by the ERC AdG CERQUTE and by the Government of Spain (Severo Ochoa CEX2019-000910-S and TRANQI), Fundació Cellex, Fundació Mir-Puig, Generalitat de Catalunya (CERCA program).

-
- [1] S. Wehner, D. Elkouss, and R. Hanson, “Quantum internet: A vision for the road ahead,” *Science*, vol. 362, no. 6412, 2018.
 - [2] S. Pirandola, “End-to-end capacities of a quantum communication network,” *Communications Physics*, vol. 2, no. 1, pp. 1–10, 2019.
 - [3] M. Pant, H. Krovi, D. Towsley, L. Tassioulas, L. Jiang, P. Basu, D. Englund, and S. Guha, “Routing entanglement in the quantum internet,” *npj Quantum Information*, vol. 5, no. 1, p. 25, 2019.
 - [4] X. Guo, C. R. Breum, J. Borregaard, S. Izumi, M. V. Larsen, T. Gehring, M. Christandl, J. S. Neergaard-Nielsen, and U. L. Andersen, “Distributed quantum sensing in a continuous-variable entangled network,” *Nature Physics*, vol. 16, no. 3, pp. 281–284, 2020.
 - [5] G. Bianconi, A. Arenas, J. Biamonte, L. D. Carr, B. Kahng, J. Kertesz, J. Kurths, L. Lü, C. Masoller, A. E. Motter, M. Perc, F. Radicchi, R. Ramaswamy, F. A. Rodrigues, M. Sales-Pardo, M. S. Miguel, S. Thurner, and T. Yasseri, “Complex systems in the spotlight: next steps after the 2021 nobel prize in physics,” *Journal of Physics: Complexity*, vol. 4, p. 010201, jan 2023.
 - [6] M. Chen, N. C. Menicucci, and O. Pfister, “Experimental realization of multipartite entanglement of 60 modes of a quantum optical frequency comb,” *Physical review letters*, vol. 112, no. 12, p. 120505, 2014.
 - [7] Y. Cai, J. Roslund, G. Ferrini, F. Arzani, X. Xu, C. Fabre, and N. Treps, “Multimode entanglement in reconfigurable graph states using optical frequency combs,” *Nature communications*, vol. 8, no. 1, pp. 1–9, 2017.
 - [8] S. Yokoyama, R. Ukai, S. C. Armstrong, C. Sornphiphatphong, T. Kaji, S. Suzuki, J.-i. Yoshikawa, H. Yonezawa, N. C. Menicucci, and A. Furusawa, “Ultra-large-scale continuous-variable cluster states multiplexed in the time domain,” *Nature Photonics*, vol. 7, no. 12, p. 982, 2013.
 - [9] W. Asavanant, Y. Shiozawa, S. Yokoyama, B. Charoensombutamon, H. Emura, R. N. Alexander, S. Takeda, J.-i. Yoshikawa, N. C. Menicucci, H. Yonezawa, *et al.*, “Generation of time-domain-multiplexed two-dimensional cluster state,” *Science*, vol. 366, no. 6463, pp. 373–376, 2019.
 - [10] M. V. Larsen, X. Guo, C. R. Breum, J. S. Neergaard-Nielsen, and U. L. Andersen, “Deterministic generation of a two-dimensional cluster state,” *Science*, vol. 366, no. 6463, pp. 369–372, 2019.
 - [11] J. Nokkala, F. Arzani, F. Galve, R. Zambrini, S. Maniscalco, J. Piilo, N. Treps, and V. Parigi, “Reconfigurable optical implementation of quantum complex networks,” *New Journal of Physics*, vol. 20, no. 5, p. 053024, 2018.
 - [12] P. Renault, J. Nokkala, G. Roeland, N. Joly, R. Zambrini, S. Maniscalco, P. Jyrki, N. Treps, and V. Parigi, “Experimental optical simulator of reconfigurable and complex quantum environment,” arXiv: 2302.12674.
 - [13] T. Kouadou, F. Sansavini, M. Ansquer, J. Henaff, N. Treps, and V. Parigi, “Spectrally shaped and pulse-by-pulse multiplexed multimode squeezed states of light,” *arXiv preprint arXiv:2209.10678*, 2022.
 - [14] L. S. Madsen, F. Laudenbach, M. F. Askarani, F. Rortais, T. Vincent, J. F. Bulmer, F. M. Miatto, L. Neuhaus, L. G. Helt, M. J. Collins, *et al.*, “Quantum computational advantage with a programmable photonic processor,” *Nature*, vol. 606, no. 7912, pp. 75–81, 2022.
 - [15] I. Suleiman, J. A. H. Nielsen, X. Guo, N. Jain, J. Neergaard-Nielsen, T. Gehring, and U. L. Andersen, “40 km fiber transmission of squeezed light measured with a real local oscillator,” *Quantum Science and Technology*, vol. 7, p. 045003, jul 2022.
 - [16] I. J. Tillman, A. Rubenok, S. Guha, and K. P. Seshadreesan, “Supporting multiple entanglement flows through a continuous-variable quantum repeater,” *Phys. Rev. A*, vol. 106, p. 062611, Dec 2022.
 - [17] J. Eisert, *Entanglement in quantum information theory*. Phd thesis, University of Postdam, 2001.
 - [18] G. Vidal and R. F. Werner, “Computable measure of entanglement,” *Phys. Rev. A*, vol. 65, p. 032314, Feb 2002.
 - [19] M. B. Plenio, “Logarithmic negativity: A full entanglement monotone that is not convex,” *Phys. Rev. Lett.*, vol. 95, p. 090503, Aug 2005.
 - [20] N. C. Menicucci, P. van Loock, M. Gu, C. Weedbrook, T. C. Ralph, and M. A. Nielsen, “Universal quantum computation with continuous-variable cluster states,” *Phys. Rev. Lett.*, vol. 97, p. 110501, Sep 2006.
 - [21] M. Gu, C. Weedbrook, N. C. Menicucci, T. C. Ralph, and P. van Loock, “Quantum computing with continuous-variable clusters,” *Physical Review A*, vol. 79, no. 6, p. 062318, 2009.
 - [22] F. Arzani, G. Ferrini, F. Grosshans, and D. Markham, “Random coding for sharing bosonic quantum secrets,” *Phys. Rev. A*, vol. 100, p. 022303, Aug 2019.

- [23] O. Pinel, J. Fade, D. Braun, P. Jian, N. Treps, and C. Fabre, “Ultimate sensitivity of precision measurements with intense gaussian quantum light: A multimodal approach,” *Phys. Rev. A*, vol. 85, p. 010101, Jan 2012.
- [24] M. Gessner, L. Pezzè, and A. Smerzi, “Sensitivity bounds for multiparameter quantum metrology,” *Phys. Rev. Lett.*, vol. 121, p. 130503, Sep 2018.
- [25] N. C. Menicucci, S. T. Flammia, and P. van Loock, “Graphical calculus for gaussian pure states,” *Physical Review A*, vol. 83, no. 4, p. 042335, 2011.
- [26] L. Lami, B. Regula, X. Wang, R. Nichols, A. Winter, and G. Adesso, “Gaussian quantum resource theories,” *Physical Review A*, vol. 98, no. 2, p. 022335, 2018.
- [27] M. Idel, D. Lercher, and M. M. Wolf, “An operational measure for squeezing,” *Journal of Physics A: Mathematical and Theoretical*, vol. 49, no. 44, p. 445304, 2016.
- [28] D. Cvetkovic, M. Doob, and H. Sachs, *Spectra of Graphs: Theory and Applications*. Wiley, 1999.
- [29] M. Van den Nest, A. Miyake, W. Dür, and H. J. Briegel, “Universal resources for measurement-based quantum computation,” *Phys. Rev. Lett.*, vol. 97, p. 150504, Oct 2006.
- [30] M. E. Newman, “The structure and function of complex networks,” *SIAM review*, vol. 45, no. 2, pp. 167–256, 2003.
- [31] F. Mascherpa, A. Smirne, A. D. Somoza, P. Fernández-Acebal, S. Donadi, D. Tamascelli, S. F. Huelga, and M. B. Plenio, “Optimized auxiliary oscillators for the simulation of general open quantum systems,” *Phys. Rev. A*, vol. 101, p. 052108, May 2020.
- [32] I. J. Farkas, I. Derényi, A.-L. Barabási, and T. Vicsek, “Spectra of “real-world” graphs: Beyond the semicircle law,” *Physical Review E*, vol. 64, no. 2, p. 026704, 2001.
- [33] I. Ispolatov, P. L. Krapivsky, and A. Yuryev, “Duplication-divergence model of protein interaction network,” *Physical review E*, vol. 71, no. 6, p. 061911, 2005.
- [34] A. Elmokashfi, A. Kvalbein, and C. Dovrolis, “On the scalability of BGP: the roles of topology growth and update rate-limiting,” in *Proceedings of the 2008 ACM CoNEXT Conference*, pp. 1–12, 2008.
- [35] E. P. Wigner, “On the distribution of the roots of certain symmetric matrices,” *Annals of Mathematics*, pp. 325–327, 1958.
- [36] P. van Loock and S. L. Braunstein, “Multipartite entanglement for continuous variables: a quantum teleportation network,” *Physical Review Letters*, vol. 84, no. 15, p. 3482, 2000.
- [37] F. Centrone, “Routing in CV-networks.” *Software Heritage repository* sw.hub.io/dirs/49a931dca9247cabcbf58a9873fa5eea6db3ce47 containing the numerical tools developed for this article, 2021.
- [38] H. Leone, N. R. Miller, D. Singh, N. K. Langford, and P. P. Rohde, “QuNet: Cost vector analysis and multi-path entanglement routing in quantum networks.” [arXiv:2105.00418](https://arxiv.org/abs/2105.00418).
- [39] C. Meignant, D. Markham, and F. Grosshans, “Distributing graph states over arbitrary quantum networks,” *Phys. Rev. A*, vol. 100, p. 052333, Nov 2019.
- [40] C. Meignant, D. Markham, and F. Grosshans, “Classical-quantum network coding: a story about tensor.” [arXiv:2104.04745](https://arxiv.org/abs/2104.04745).
- [41] B. Zhang and Q. Zhuang, “Entanglement formation in continuous-variable random quantum networks,” *npj Quantum Information*, vol. 7, no. 1, p. 33, 2021.
- [42] Q. Zhuang and B. Zhang, “Quantum communication capacity transition of complex quantum networks,” *arXiv preprint arXiv:2011.07397*, 2020.
- [43] Y. Omar, J. Moutinho, A. Melo, B. Coutinho, I. Kovacs, and A. Barabási, “Quantum link prediction in complex networks,” in *APS March Meeting Abstracts*, vol. 2019, pp. R28–003, 2019.
- [44] M. Cuquet and J. Calsamiglia, “Limited-path-length entanglement percolation in quantum complex networks,” *Physical Review A*, vol. 83, no. 3, p. 032319, 2011.
- [45] C. Harney and S. Pirandola, “Analytical methods for high-rate global quantum networks,” *PRX Quantum*, vol. 3, no. 1, p. 010349, 2022.
- [46] N. R. Solomons, A. I. Fletcher, D. Aktas, N. Venkatachalam, S. Wengerowsky, M. Lončarić, S. P. Neumann, B. Liu, Ž. Samec, M. Stipčević, *et al.*, “Scalable authentication and optimal flooding in a quantum network,” *PRX Quantum*, vol. 3, no. 2, p. 020311, 2022.
- [47] S. K. Joshi, D. Aktas, S. Wengerowsky, M. Lončarić, S. P. Neumann, B. Liu, T. Scheidl, G. C. Lorenzo, Ž. Samec, L. Kling, *et al.*, “A trusted node-free eight-user metropolitan quantum communication network,” *Science advances*, vol. 6, no. 36, p. eaba0959, 2020.
- [48] F. Hahn, A. Pappa, and J. Eisert, “Quantum network routing and local complementation,” *npj Quantum Information*, vol. 5, no. 1, p. 76, 2019.
- [49] J. Roslund, R. M. De Araujo, S. Jiang, C. Fabre, and N. Treps, “Wavelength-multiplexed quantum networks with ultrafast frequency combs,” *Nature Photonics*, vol. 8, no. 2, p. 109, 2014.
- [50] H. Yonezawa, T. Aoki, and A. Furusawa, “Demonstration of a quantum teleportation network for continuous variables,” *Nature*, vol. 431, no. 7007, pp. 430–433, 2004.
- [51] C. Fabre and N. Treps, “Modes and states in quantum optics,” *Reviews of Modern Physics*, vol. 92, no. 3, p. 035005, 2020.
- [52] V. Roman-Rodriguez, B. Brecht, K. Srinivasan, C. Silberhorn, N. Treps, E. Diamanti, and V. Parigi, “Continuous variable multimode quantum states via symmetric group velocity matching,” *New Journal of Physics*, vol. 23, no. 4, p. 043012, 2021.
- [53] A. Christ, C. Lupo, M. Reichelt, T. Meier, and C. Silberhorn, “Theory of filtered type-II parametric down-conversion in the continuous-variable domain: Quantifying the impacts of filtering,” *Physical Review A*, vol. 90, no. 2, p. 023823, 2014.
- [54] F. Arzani, C. Fabre, and N. Treps, “Versatile engineering of multimode squeezed states by optimizing the pump spectral profile in spontaneous parametric down-conversion,” *Physical Review A*, vol. 97, no. 3, p. 033808, 2018.
- [55] E. Gouzien, S. Tanzilli, V. d’Auria, and G. Patera, “Morphing supermodes: A full characterization for enabling multimode quantum optics,” *Physical Review Letters*, vol. 125, no. 10, p. 103601, 2020.
- [56] M. Yukawa, R. Ukai, P. Van Loock, and A. Furusawa, “Experimental generation of four-mode continuous-variable cluster states,” *Physical Review A*, vol. 78, no. 1, p. 012301, 2008.
- [57] D. Barral, M. Walschaers, K. Bencheikh, V. Parigi, J. A. Levenson, N. Treps, and N. Belabas, “Versatile photonic entanglement synthesizer in the spatial domain,” *Physical Review Applied*, vol. 14, no. 4, p. 044025, 2020.
- [58] J. Arrazola, V. Bergholm, K. Brádler, T. Bromley, M. Collins, I. Dhand, A. Fumagalli, T. Gerrits, A. Goussev, L. Helt, *et al.*, “Quantum circuits with many photons

- on a programmable nanophotonic chip,” *Nature*, vol. 591, no. 7848, pp. 54–60, 2021.
- [59] M. Walschaers, N. Treps, S. Bhuvanesh, L. D. Carr, and V. Parigi, “Emergent complex quantum networks in continuous-variables non-Gaussian states.” arXiv:2012.15608.
- [60] A. E. Brouwer and W. H. Haemers, *Spectra of graphs*. Springer Science & Business Media, 2011.
- [61] M. E. J. Newman, *Networks, second edition*. Oxford University Press, 2018.
- [62] A. L. Barabási, *Networks science*. Cambridge University Press, 2016.
- [63] P. Erdos, A. Rényi, *et al.*, “On the evolution of random graphs,” *Publ. Math. Inst. Hung. Acad. Sci.*, vol. 5, no. 1, pp. 17–60, 1960.
- [64] D. J. Watts and S. H. Strogatz, “Collective dynamics of ‘small-world’ networks,” *nature*, vol. 393, no. 6684, pp. 440–442, 1998.
- [65] R. Albert and A.-L. Barabási, “Statistical mechanics of complex networks,” *Reviews of modern physics*, vol. 74, no. 1, p. 47, 2002.
- [66] S. Pirandola and S. Mancini, “Quantum teleportation with continuous variables: A survey,” *Laser Physics*, vol. 16, no. 10, pp. 1418–1438, 2006.
- [67] C. Weedbrook, S. Pirandola, R. García-Patrón, N. J. Cerf, T. C. Ralph, J. H. Shapiro, and S. Lloyd, “Gaussian quantum information,” *Rev. Mod. Phys.*, vol. 84, pp. 621–669, May 2012.
- [68] R. Simon, “Peres-horodecki separability criterion for continuous variable systems,” *Physical Review Letters*, vol. 84, no. 12, p. 2726, 2000.
- [69] N. Acosta-Mendoza, A. Gago-Alonso, and J. E. Medina-Pagola, “Frequent approximate subgraphs as features for graph-based image classification,” *Knowledge-Based Systems*, vol. 27, pp. 381–392, 2012.
- [70] O. Jones, “Spectra of simple graphs,” *Whitman College, Walla-Walla*, 2013.

VII. COMPETING INTERESTS

The Authors declare no Competing Financial or Non-Financial Interests.

VIII. DATA AVAILABILITY

The numerical data that support the finding are available from the authors upon request and can be reproduced using the repository [37].

IX. AUTHOR CONTRIBUTIONS

F.C. operated the numerical simulations and analyzed the data. All authors contributed to the theoretical analysis and to writing the manuscript. V.P and F.C. supervised the work. V.P conceived the project.

Appendix A: Squeezing spectra of regular graphs

Given any graph’s spectrum we can employ equation (2) to compute the amount of squeezing in each mode

required to build the Gaussian network. In the following calculations we used the spectra of regular graphs known in literature. A detailed reference on the spectra of regular graphs and how to obtain them can be found here [60, 70].

We use the linear graph as a benchmark to see how the squeezing cost scales with the number of nodes and links. In fact, single mode squeezing and the CZ-gate both require a fixed amount of squeezing to be implemented, so we would expect $G(\sigma)$ to scale linearly with the number of links and nodes. This is a direct consequence of the spectral distribution of the linear graph, which is

$$D_k(\mathcal{L}_N) = 2g \cos \frac{\pi k}{N+1}, \{k = 1, \dots, N\}. \quad (\text{A1})$$

We can use equations (2) and (3) to compute the squeezing cost exactly for any given N . For $N \gg 1$, the sum in Eq. (3) allowing to compute the average squeezing cost per mode $\bar{G} = G/(\text{\#squeezed modes}) = G/\text{rk}(A)$ can be seen as a Riemann integral, which converges to

$$\bar{G} \simeq 10 \int_0^1 \log_{10} \left[1 + \frac{g^2 \cos^2 \pi y^2}{2} + \sqrt{g^2 \cos^2 \pi y + \frac{g^4 \cos^4 \pi y}{4}} \right] dy \quad (\text{A2})$$

This can be easily generalized to the case of a D -dimensional cubic lattice $\mathcal{L}_N^{(D)}$, considering that adding a new dimension would just add a new set of eigenvalues of the form (A1), as shown in section 2.6 of [28]. As a consequence, the squeezing cost of the $\mathcal{L}_N^{(D)}$ is $G = O(N^D)$, whereas the average cost per mode would be again constant with the number of nodes N , as shown in Fig. 10.

Similarly, we can use the eigenvalues expression of the circular graph (or its generalization with $Q > 1$ nearest neighbors)

$$D_k(\mathcal{G}_{C(Q)}) = g \frac{\sin[(Q+1)k\pi/N]}{\sin[k\pi/N]} - g, \quad k = \{0, \dots, N-1\}. \quad (\text{A3})$$

From this we can see why the linear and circular graph have the same scaling. In fact for $Q = 1$, we have $D_k(\mathcal{G}_{C(Q)}) = 2g \cos(k\pi/N) - g$.

The spectra of the star and diamond graph have only two non-null eigenvalues [70]

$$\{D_k(\mathcal{S}_N)\} = \left\{ g\sqrt{N-1}, 0^{\otimes(N-2)}, -g\sqrt{N-1} \right\}, \quad (\text{A4})$$

$$\{D_k(\mathcal{D}_N)\} = \left\{ g\sqrt{2N}, 0^{\otimes(N-2)}, -g\sqrt{2N} \right\}. \quad (\text{A5})$$

As a consequence, the cost of the star and diamond Gaussian networks grows logarithmically with N and have the following expressions.

$$G(\sigma_{\mathcal{S}_N}) = 20 \log_{10} \frac{2 - g^2 + g^2 N + \sqrt{g^4 N^2 - 2(2g^4 - g^2)N + g^4 - 4g^2}}{2} \quad (\text{A6})$$

$$= 20 \log_{10} N + 20 \log g^2 + O\left(\frac{1}{N}\right); \quad (\text{A7})$$

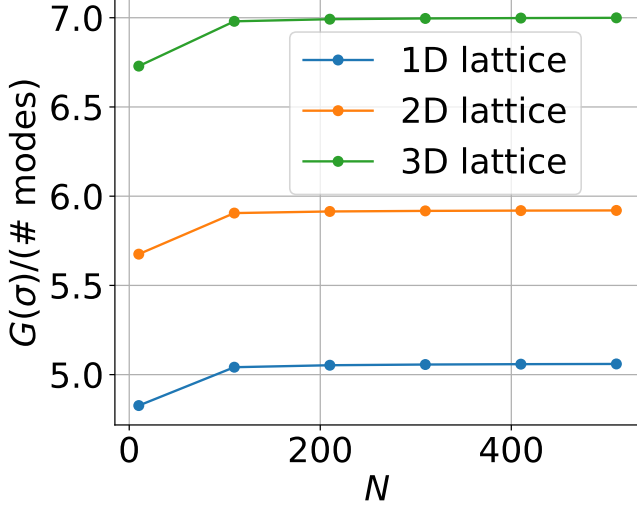


FIG. 10: Trend of the average squeezing cost per mode $\bar{G}(\sigma)$ for 1D, 2D and 3D lattices, with N , N^2 and N^3 nodes respectively. Notice that the cost becomes asymptotically constant, as predicted by the theory.

$$G(\sigma_{\mathcal{D}_N}) = 20 \log_{10} \left(1 + g^2 N + g \sqrt{N(g^2 N + 4)} \right) \quad (\text{A8})$$

$$= 20 \log_{10} N + 20 \log_{10} 2g^2 + O\left(\frac{1}{N}\right). \quad (\text{A9})$$

Finally, the spectrum of the fully connected graph is

$$\{D_k(\mathcal{S}_N)\} = \{g(N-1), -g^{\otimes(N-1)}\}, \quad (\text{A10})$$

yielding a squeezing cost that can be expressed as the sum of two contributions

$$G(\sigma_{\mathcal{F}_N}) = 10(N-1) \log_{10} \frac{2+g^2+g\sqrt{g^2+4}}{2} + 10 \log_{10} \left[1 + \frac{1 + \sqrt{1 + \frac{4}{g^2(N-1)^2}}}{2} g^2 (N-1)^2 \right] \quad (\text{A11})$$

$$= 10(N-1) \log_{10} \frac{2+g^2+g\sqrt{g^2+4}}{2} + 20 \log_{10} N + 20 \log_{10} g + O\left(\frac{1}{N}\right), \quad (\text{A12})$$

which sums up to a cost growing essentially linearly in N .

Appendix B: Squeezing spectrum of Erdős–Rényi graphs

From Fig. 4 we notice that the most expensive growth belongs to the ER topology, which is the only one among the topologies we studied whose trend is super-linear. This behaviour is actually the easiest to predict from random matrix theory: the Wigner semi-circular law for the distribution of the eigenvalues of a random graph [35] gives their probability distribution in the form $f(x) = f_{ER}(x) = \frac{2}{\pi R^2} \sqrt{R^2 - x^2}$ (see Fig. 9a), where $R = 2g\sqrt{Np(1-p)}$, with a supplementary large eigenvalue D_1 such that $\lim_{N \rightarrow \infty} D_1/gN = p$, with probability 1. Casting it in equation (4) gives

$$\langle G(\sigma_{ER}) \rangle = 10 \log_{10} [2\lambda^+(gpN)] \quad (\text{B1})$$

$$+ \frac{40N}{\pi R^2} \int_0^R \sqrt{R^2 - x^2} \log_{10} (2\lambda^+(x)) dx,$$

where we used the parity of $f_{ER}(x)$, and the fact that the support is in $[0, R]$. Figure 11 shows the comparison between the theoretical behaviour of the squeezing cost of the ER graph and the numerical experiments from the simulations. It shows a superlinear $\propto N \log N$ increase of the squeezing cost, which is explained by the widening of the support of f due to the increasing values of R . More formally, making the variable change $x = Ry$, we have

$$\log_{10} (2\lambda^+(Ry)) = 2 \log_{10} R + \log_{10} \frac{y^2}{2} + O\left(\frac{1}{R^2 y^2}\right). \quad (\text{B2})$$

The second term in eq. (B1) then becomes

$$\begin{aligned} & \frac{40N}{\pi} \int_0^1 \sqrt{1-y^2} \log_{10} (\lambda^+(Ry)) dy \\ &= \frac{80N \log_{10}(R)}{\pi} \int_0^1 \sqrt{1-y^2} dy + O(N) \\ &= 10N \log_{10}(g^2 N p(1-p)) + O(N), \end{aligned} \quad (\text{B3})$$

and is the dominant term in the squeezing cost.

Appendix C: Graphical Calculus

In Ref. [25] Menicucci, Flammia and van Loock is provide a unified graphical calculus for all Gaussian pure states which is particularly suited for describing highly multimode Gaussian networks.

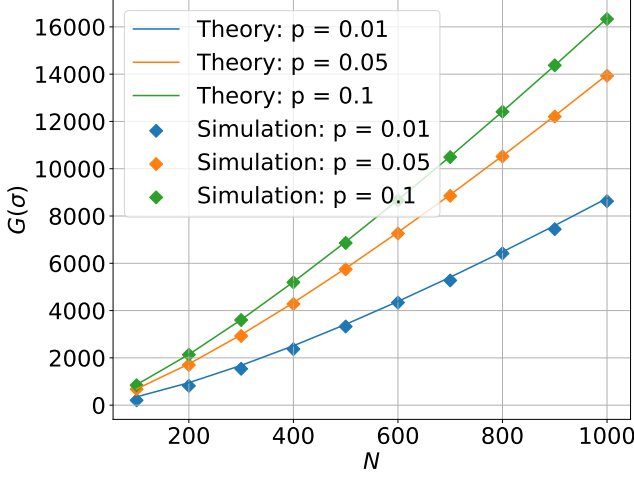


FIG. 11: Comparison between the theoretical prediction of equation (4) and the experimental numerical simulation of the squeezing cost of the Erdős-Rényi graph state, for different values of p .

In this framework, a N mode Gaussian state is completely described, up to displacements, by a $N \times N$ complex valued adjacency matrix:

$$Z = V + iU \quad (C1)$$

Where the real and imaginary part of Z , V and U respectively, are related to the covariance matrix through the following unique decomposition

$$\sigma = \frac{1}{2} \begin{pmatrix} U^{-1} & U^{-1}V \\ VU^{-1} & U + VU^{-1}V \end{pmatrix} \quad (C2)$$

Gaussian graph states have a particular simple graphical representation, being

$$Z = A + iD \quad (C3)$$

Where A is the weighted adjacency matrix of the graph and D is a diagonal matrix that represents momentum squeezing, i.e. for $D = 10^{-2s/10}\mathbb{1}$ the momentum variance of all modes is reduced by $2s$ decibels.

All symplectic operations can be reproduced in this language, however, since we already know how to represent the resource graph states, we only need to implement the quadrature measurements in \hat{x} and \hat{p} . We can express the state as

$$Z = \begin{pmatrix} t & RR^T \\ R & W \end{pmatrix} \quad (C4)$$

Where the scalar t is the target mode we want to measure, $W \in \mathbb{R}^{(N-1) \times (N-1)}$ is the subgraph of the untouched modes and $R \in \mathbb{R}^{(N-1) \times 1}$ their correlations with the target mode. We have the following two rules:

- $Z \rightarrow Z_q = W$ after a \hat{q} measurement.
- $Z \rightarrow Z_p = W - \frac{RR^T}{t}$ after a \hat{p} measurement.

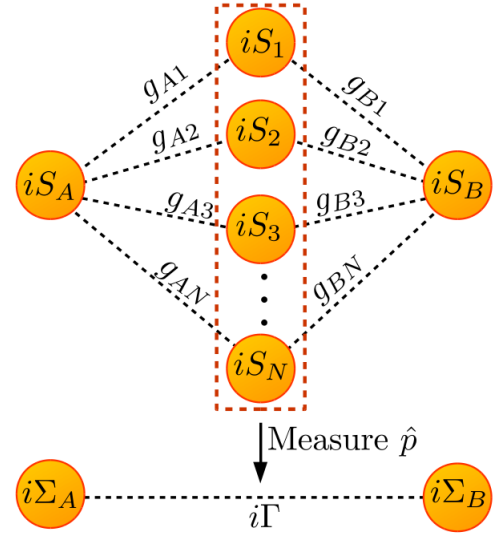


FIG. 12: Graphical representation of the diamond graph and its parallel enhancement of entanglement.

Thus, for a measurement in \hat{q} we simply remove the node and its links from the graph, whereas for a measurement in \hat{p} we also change the correlation between its neighbors, since $(RR^T)_{ij} \neq 0$ iff both i and j are in the node's neighborhood.

Appendix D: Parallel enhancement of entanglement

We can use the rules described in Appendix C to prove eq. (5), which expresses analytically the power of parallel enhancement of entanglement in the diamond network when measuring the central nodes in \hat{p} . Let us assume that the nodes A and B are squeezed by a factor S_A and S_B respectively, there are N central nodes and the k th mode has squeezing S_k and is correlated with A and B through a CZ-gate with strength g_{Ak} and g_{Bk} . It can then be easily showed that the final pair will have a purely imaginary adjacency matrix of the form

$$Z_{AB} = i \begin{pmatrix} \Sigma_A & \Gamma \\ \Gamma & \Sigma_B \end{pmatrix} \quad (D1)$$

Where $\Sigma_A = S_A + \sum_k \frac{g_{Ak}^2}{S_k}$, $\Sigma_B = S_B + \sum_k \frac{g_{Bk}^2}{S_k}$ and $\Gamma = \sum_k \frac{g_{Ak}g_{Bk}}{S_k}$. These result can be derived by direct application of the rule for measuring \hat{p} in the graphical calculus formalism, schematized in figure 12.

Employing eqs. (C1) and (C2) and noticing that $V = 0$, we can reconstruct the covariance matrix of the final pair:

$$\sigma_f = \begin{pmatrix} \frac{\Sigma_B}{\Sigma_A \Sigma_B - \Gamma^2} & -\frac{\Gamma}{\Sigma_A \Sigma_B - \Gamma^2} & 0 & 0 \\ -\frac{\Gamma}{\Sigma_A \Sigma_B - \Gamma^2} & \frac{\Sigma_A}{\Sigma_A \Sigma_B - \Gamma^2} & 0 & 0 \\ 0 & 0 & \Sigma_A & \Gamma \\ 0 & 0 & \Gamma & \Sigma_B \end{pmatrix} \quad (D2)$$

Notice that this state differs from a graph state by a local phase.

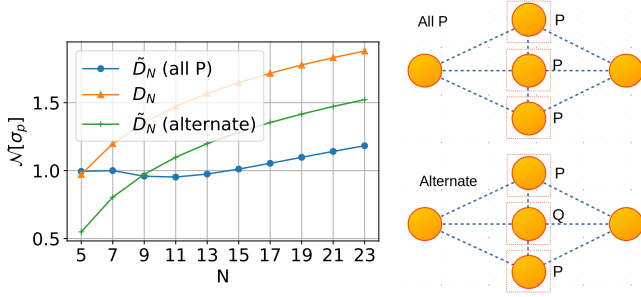


FIG. 13: Different measurement strategies for two types of diamond network: the standard \mathcal{D}_N we have seen so far and the $\tilde{\mathcal{D}}_N$, in which the central nodes are connected to their neighbors. We apply two different strategies to $\tilde{\mathcal{D}}_N$: one is to measure all the central nodes in P and the other is to alternate a p and a q measurement. We can see that measuring always in p is not necessarily the optimal strategy. On the right side you can see a scheme of the $\tilde{\mathcal{D}}$ network and the two different measurement strategies.

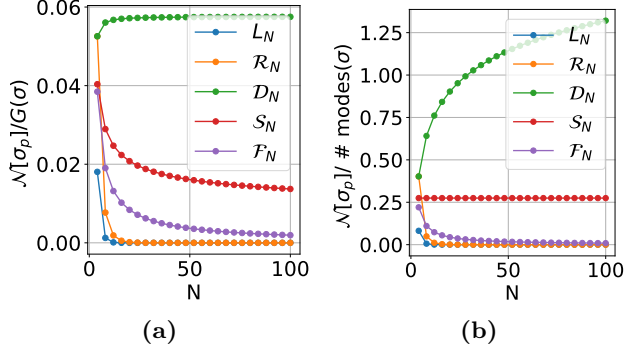


FIG. 14: Trend of the ratio between the logarithmic negativity of the final state and (a) the squeezing cost of the initial state or (b) the total number of modes in the initial state for regular topologies: linear \mathcal{L}_N , ring \mathcal{R}_N , star \mathcal{S}_N , diamond \mathcal{D}_N , and fully connected \mathcal{F}_N networks up to $N = 100$ nodes.

By computing the seralian — defined in Eq. (15) — of the partially transpose covariance matrix of the pair $\tilde{\sigma}_f$ and applying formula (16), we obtain the general lowest symplectic eigenvalue of the partial transpose of the state

$$\nu_-^2 = \frac{(\sqrt{\Sigma_A \Sigma_B} - \Gamma)^2}{\Sigma_A \Sigma_B - \Gamma^2} \quad (\text{D3})$$

Finally, if we assume that all the modes are equally squeezed in \hat{p} of a factor $R^{-1} = 10^{2s/10}$ and all the CZ-gate correlations have a strength g , we arrive to Eq. (5).

This property of the Diamond network, however, is not easily generalized to all graphs that present parallel connections and the quest for the optimal measurement strategy in order to improve the final entanglement is by no means trivial. This is the case, for example, of the $\tilde{\mathcal{D}}$ graph shown in Fig. 13, generated by taking the diamond network and add a CZ-gate link between adjacent central nodes. We can see that for $N > 9$ always measuring \hat{p} in this network is not the optimal strategy, whereas a better strategy is to alternate a \hat{p} and \hat{q} measurement in order

to restore a (smaller) diamond network.

Another important figure of merit is the entanglement per squeezing cost, shown in Fig 14 (a).

We see that the diamond is the only one that gives the a ratio of entanglement per cost of the network that becomes constant for large N . However, the linear graph is the one that links two nodes that are the furthest away from each other. Conversely, figure 14 (b) shows the logarithmic negativity in the final pair divided by the number of modes in the initial state. Once again, the diamond structure is particularly convenient, yielding the highest logarithmic negativity while keeping a constant number of independent squeezers.

In order to give a fair comparison between the capacity of the linear network to bridge distant nodes and that of the diamond to increase the final entanglement we need to generalize the diamond graph to a diamond chain graph, $\mathcal{DC}_{K,N}$, where K is the number of parallel branches linking the two hubs that want to perform quantum communications as in figure 15.

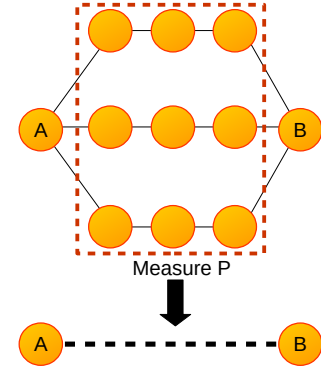


FIG. 15: Scheme of an entanglement routing protocol in a diamond chain with $K=3$. All the central nodes are measured in P in order to concentrate entanglement between Alice and Bob.

We can then compare the entanglement concentrated using multiple path strategies to link two nodes far away from each other. We can see in figure 16 that the presence of parallel links has indeed the desired effect, despite the quality of the final pair, which still decreases exponentially with the distance. On the other hand, notice that the parallel links can help concentrating more entanglement until the system reaches a plateau and even the additional channels will not allow to increase the logarithmic negativity. Moreover, the value for effort of this networks, specifically the ratio between the entanglement of the pair after the protocol and the squeezing cost before the protocol, is maximized by the linear graph.

Another important class of networks, notably for measurement based quantum computation, is constituted by grid cluster states that belong to graph shapes that allow for universal quantum computation [29]. Similarly to the diamond network, the presence of ancillary nodes between the emitter and the receiver can improve the quality of the quantum link with respect to the linear network. This,

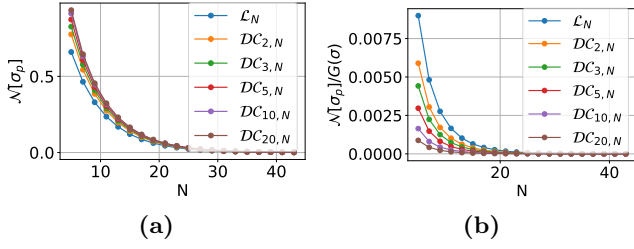


FIG. 16: (a) Trend of the logarithmic negativity of the output state for the diamond chain network, for various values of the number of branches K ($K=1$ is the linear network). (b) Trend of the ratio between the logarithmic negativity of the final state and the squeezing cost of the initial state for the diamond chains.

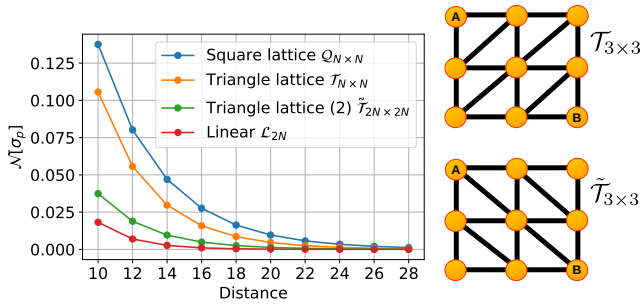


FIG. 17: Comparison between the entanglement capacity between two nodes at the same distance of three lattices graphs, the square lattice $Q_{N \times N}$ and the two triangles $T_{N \times N}$, formed from the square by adding edges on the diagonals in such a way that the distance between A and B is the same, $\tilde{T}_{N \times N}$ formed by adding edges to the diagonals so that the distance is the same as the linear graph, and the linear graph L_N . In order to compare the networks with the same distance we doubled the size of the \tilde{T} and the L graphs.

however, is not a general rule and sometimes the presence of additional links can be detrimental. This is the case of the triangular lattice, generated from the square lattice by adding a link between the nodes in the diagonal. There are two ways of generating the triangular and only one of the two, \tilde{T} , decreases effectively the distance between Alice and Bob. In both cases the result is detrimental, however \mathcal{T} is slightly better than $\tilde{\mathcal{T}}$, while the square lattice \mathcal{Q} seems to be the most effective. This result is shown in figure 17.

Appendix E: Routing in complex networks

The same analysis of section II B 2 was done in several networks with different sizes and topologies with very different results that we report in figures 18, 19, 20 and 21. A property that is not apparent in Fig. 8, is that the node with the highest enhancement of entanglement due to the multiple paths is not necessarily the one with the highest logarithmic negativity in absolute. This is the case of the ER network of Fig. 18, in which the node with the highest entanglement, highlighted in green in the graph representation, is at distance 1 while the node with the highest difference in logarithmic negativity between the *Routing* and the *Shortest* protocols, highlighted in red, is at distance 3. In this case, the structure of the subgraph used throughout the *Routing* is not a diamond chain and the intercorrelations among the parallel branches have limited the increase of the entanglement, as for the $\tilde{\mathcal{D}}_N$ network in Fig. 13. In any case, in this network the nodes at greater distances are the ones that are most affected by our protocol and, although in some cases many parallel paths have been disregarded, as shown by the height of the grey column, all the nodes at distance 4 received a substantial enhancement.

The results of the simulation on the BA topology of Fig. 19 is similar to the AS, although the first only reaches a distance of 3. The nodes with the highest absolute logarithmic negativity and the highest logarithmic negativity difference produced by the *Routing* protocol coincide and are at distance 2 from Alice, whereas this time the subgraph of is a diamond with no interconnections. Also in this case distance 2 is favorable to perform quantum communications.

The WS structure of Fig. 20, on the other hand, is the worst to apply the *Routing* protocol. Only a few nodes, in fact, were poorly enhanced and mostly at large distances, while the logarithmic negativity averaged over all the nodes for *Routing* and *Shortest* is comparable. The node 44 at distance 3 is the one that received the greatest boost from our protocol, whereas node 1 (like all the other nodes at distance 1) has the highest logarithmic negativity.

Finally, the biological network of Fig. 21 produced the most interesting results. Once again, many nodes at distance 2 end up having more logarithmic negativity than those at distance 1, and at this distance the nodes with the same degree have the same logarithmic negativity that decreases exponentially with their degree. The nodes with highest logarithmic negativity and highest difference coincide with node 139, which is linked to Alice through 33 intermediate nodes, forming a diamond network with no interconnections.

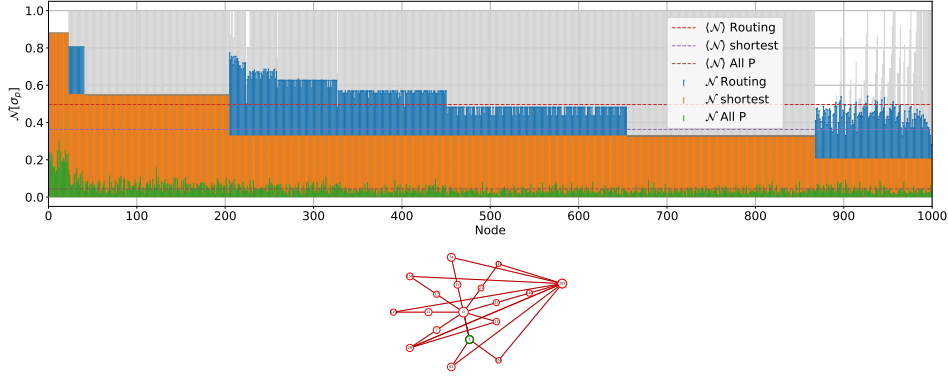


FIG. 18: Logarithmic negativity produced by the three different protocols applied to each node of the $\mathcal{G}_{ER}(N=1000, p=0.4)$ network.

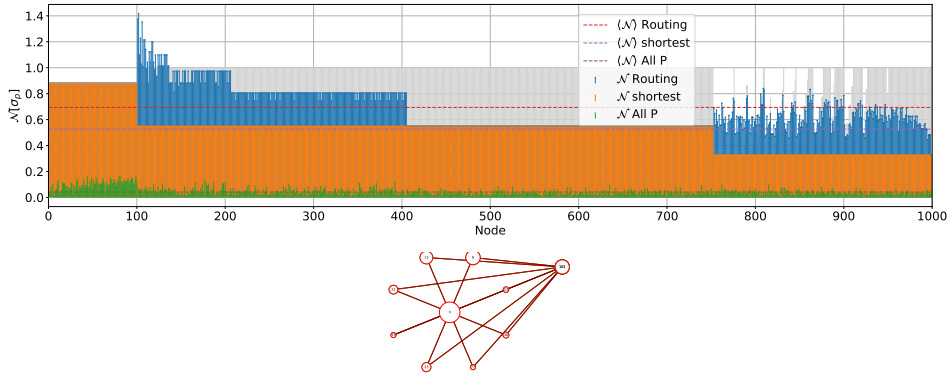


FIG. 19: Logarithmic negativity produced by the three different protocols applied to each node of the $\mathcal{G}_{BA}(N=1000, K=4)$ network.

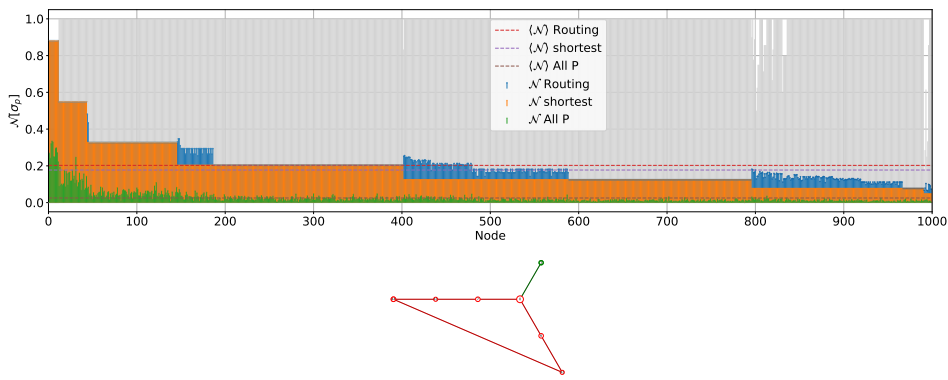


FIG. 20: Logarithmic negativity produced by the three different protocols applied to each node of the $\mathcal{G}_{WS}(N=1000, Q=4, \beta=0.9)$ network.

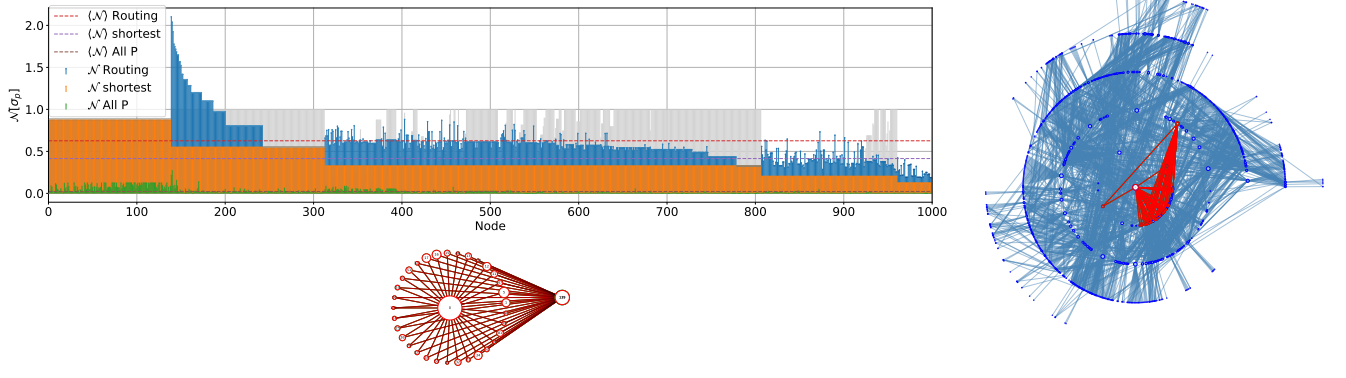


FIG. 21: Logarithmic negativity produced by the three different protocols applied to each node of the $\mathcal{G}_{PP}(N = 1000, \sigma = 0.4)$ network.